

Science with the TianQin Observatory: Preliminary Results on Stochastic Gravitational-Wave Background

Zheng-Cheng Liang,^{1,2,*} Yi-Ming Hu,^{2,†} Yun Jiang,^{2,3,‡} Jun Cheng,^{2,§} Jian-dong Zhang,^{2,¶} and Jianwei Mei^{2,**}

¹MOE Key Laboratory of Fundamental Physical Quantities Measurements, Hubei Key Laboratory of Gravitation and Quantum Physics, School of Physics, Huazhong University of Science and Technology, Wuhan 430074, China

²MOE Key Laboratory of TianQin Mission, TianQin Research Center for Gravitational Physics & School of Physics and Astronomy, Frontiers Science Center for TianQin, CNSA Research Center for Gravitational Waves, Sun Yat-sen University (Zhuhai Campus), Zhuhai 519082, China

³Max-Planck-Institut für Kernphysik, Saupfercheckweg 1, 69117 Heidelberg, Germany

(Dated: July 20, 2021)

In this work, we study the prospect of detecting the stochastic gravitational-wave background with the TianQin observatory. We consider both astrophysical-origin and cosmological-origin sources, including stellar-mass binary black holes, binary neutron stars, Galactic white dwarves, inflation, first order phase transition, and cosmic defects. For the detector configurations, we considered TianQin, TianQin I+II and TianQin + LISA. We studied the detectability of stochastic gravitational-wave backgrounds with the assumed methods of both cross-correlation and null channel, and present the corresponding power-law integrated sensitivity curves. We introduce the definition of the “joint foreground” with a network of detectors. With the joint foreground, the number of resolved double white dwarves in the Galaxy will be increased by 5% ~ 22% compared with simple combination of individual detectors. The astrophysical background from the binary black holes and the binary neutron stars under the theoretical models are predicted to be detectable with signal-to-noise ratio of around 10 after five years operation. As for the cosmological sources, their models are highly uncertain, and we only roughly estimate the detection capability under certain cases.

I. INTRODUCTION

The gravitational-wave (GW) emission from a large number of independent and unresolvable sources can not be detected individually by the GW detectors. Nevertheless, their incoherent superposition would form a stochastic GW background (SGWB), which could be detected as a bulk [1–3]. Many different mechanisms can contribute to the SGWB, by which the SGWB can be roughly divided into two categories: astrophysical-origin and cosmological-origin [4, 5].

The astrophysical SGWB mainly contains the GW emission from plenty of compact binaries [6]. For space-borne GW detectors, such source could be double white dwarfs (DWDs) [7, 8], massive black hole binaries (MBHBs) [9], stellar-mass binary black holes (SBBHs) [10], and extreme-mass-ratio inspirals (EMRIs) [11, 12]. On the other hand, the cosmological SGWB for space-borne GW detectors contains the GWs from physical processes linked to the early Universe, like the inflation [13], first order phase transition (PT) [14] and cosmic defects [15]. A detection of the SGWB would have important implications in either astrophysics or cosmology on the fundamental physics. When exploring the SGWB of extragalactic compact binaries, one can limit

the event rate, mass distribution and formation mechanisms [16–18]. As for the DWDs in the Galaxy, one can study the spatial structure by its anisotropy [19]. In addition, some physical pictures of the early Universe may be hidden in the cosmological SGWBs [20–22].

Specifically, the collection of Galaxy DWDs could exceed the noise level of space-borne GW detectors [23]. Instead of forming a background, such signal is generally classified as a *foreground* [24–27]. The capability to detect the other isotropic SGWB would not be significantly weakened when the foreground is suitably modeled [28]. Since the strength of foreground is comparable with the detector noise, in the process of data analysis for other signals, the all-sky integrated foreground could be treated as a part of the noise [29–34].

There exist a few programs for the space-borne GW detectors [6, 35–38]. In this work, we constrain our focus on TianQin [35, 39, 40] (and LISA [6] when a network is considered). TianQin is expected to explore GW astronomy as well as fundamental physics during its operation [8–12, 41, 42]. For such detectors, the laser interferometry is used to combine three satellites into a six-link triangle GW detector, with which one can build up three independent data channels. A link is formed when the laser emitted from one satellite is received by the other, which is further used to construct an interferometer.

When extracting the GW from the resolved sources such as SBBHs, a common practice is to use the matched filter method [43, 44], where a template bank with various waveforms are used to compare with the data. However, due to the stochastic nature, the SGWB has no definite waveforms. Thus, in the realm of SGWB detection, the optimal filter method is used instead [45].

* zhchliang@hust.edu.cn

† huyiming@sysu.edu.cn

‡ jiangyun5@sysu.edu.cn

§ chengj79@mail2.sysu.edu.cn

¶ zhangjd9@sysu.edu.cn

** meijw@sysu.edu.cn

For the space-borne GW missions, the laser phase noise is usually orders of magnitude higher than other noises, while the time delay interferometer (TDI) can beat down such laser phase noise [46–50]. The outcome, however, is that instead of the Michelson channel, analysis should be performed on the TDI channels, among which the A and E channels are conventional channels, while the T channel is signal-insensitive, and is also referred to as the *null channel* or *noise monitoring channel*.

In the search of SGWB, one could cross-correlate the outputs from multiple channels [51–53]. At the first glance, such method could in principle be applied to the A/E channels. However, the GW signals projected to the A and E channels belong to orthogonal polarizations. Therefore, cross correlation method can not be applied on the TDI channels [54]. Fortunately, the T channel can provide information about the noise spectrum, and the SGWB can be identified in the A and E channels with the comparison of the T channel through the *null channel* method [55, 56]. We calculate the responses of SGWB under different configurations with both the cross-correlation and null channel methods, as well as the spectra from various types of sources.

The outline of the paper is as follows. In Sec. II, we review the fundamental for the SGWB to provide a theoretical framework for the following calculation. In Sec. III, we introduce the methodology to realize the detection for the SGWB and show the power-law integrated (PI) sensitivity curves for the different configurations. In Sec. IV, we analyze the SGWBs from different origins. We summarize the conclusions in Sec. V.

II. BASIC DEFINITIONS

A. Fundamentals of SGWB

The strength of SGWB is described by the ratio of SGWB energy density per logarithmic frequency bin to the critical density of the Universe $\rho_c \equiv 3H_0^2 c^2 / (8\pi G)$ [57, 58]:

$$\Omega_{\text{gw}}(f) = \frac{1}{\rho_c} \frac{d\rho_{\text{gw}}}{d(\ln f)}. \quad (1)$$

Here $d\rho_{\text{gw}}$ is the SGWB energy density in the frequency band $[f, f + df]$, H_0 is the Hubble constant, where c is the light speed and G is the gravitational constant. In this work, we adopt $H_0 = 67.4 \text{ km s}^{-1} \text{ Mpc}^{-1}$ [59]. The overall fractional density Ω_{gw} of SGWB is given by:

$$\Omega_{\text{gw}} = \int_0^\infty d(\ln f) \Omega_{\text{gw}}(f). \quad (2)$$

The energy density is related to the metric perturbation $h_{ab}(t, \vec{x})$ [60]:

$$\rho_{\text{gw}} = \frac{c^2}{32\pi G} \langle \dot{h}_{ab}(t, \vec{x}) \dot{h}^{ab}(t, \vec{x}) \rangle, \quad (3)$$

where $\langle \dots \rangle$ denotes ensemble average [61]. In the plane wave expansion, the metric perturbation can be expressed as [62, 63]:

$$h_{ab}(t, \vec{x}) = \int_{-\infty}^{\infty} df \int_{S^2} d\Omega_{\hat{k}} \tilde{h}_{ab}(f, \hat{k}) e^{i2\pi f(t - \hat{k} \cdot \vec{x}/c)}, \quad (4)$$

where $\tilde{h}_{ab}(f, \hat{k}) = \sum_{P=+, \times} \tilde{h}_P(f, \hat{k}) e_{ab}^P(\hat{k})$, with $e_{ab}^P(\hat{k})$ being the polarization tensor [58, 64, 65].

The detector response can be expressed as the convolution of metric perturbations $h_{ab}(t, \vec{x})$ and the impulse response of the detector $\mathbb{F}^{ab}(t, \vec{x})$ [66]: $h(t) = \mathbb{F}^{ab}(t, \vec{x}) * h_{ab}(t, \vec{x})$, through which the output in the frequency-domain is derived:

$$\tilde{h}(f) = \int_{S^2} d\Omega_{\hat{k}} \sum_{P=+, \times} F^P(f, \hat{k}) \tilde{h}_P(f, \hat{k}) e^{-i2\pi f \hat{k} \cdot \vec{x}/c}, \quad (5)$$

where $F^P(f, \hat{k}) = e_{ab}^P(\hat{k}) F^{ab}(f, \hat{k})$ and

$$F^{ab}(f, \hat{k}) = e^{-i2\pi f \hat{k} \cdot \vec{x}/c} \int_{-\infty}^{\infty} d\tau \int d^3y \mathbb{F}^{ab}(\tau, \vec{y}) \times e^{-i2\pi f(\tau - \hat{k} \cdot \vec{y}/c)}. \quad (6)$$

Taking the Michelson channel as an example, we have

$$F_M^{ab}(f, \hat{k}) = \frac{1}{2} (u_1^a u_1^b \mathcal{T}(f, \hat{u}_1, \hat{k}) - u_2^a u_2^b \mathcal{T}(f, \hat{u}_2, \hat{k})), \quad (7)$$

where \hat{u}_i are the unit vectors for the two arms of the Michelson channel and u_i^a denotes the a -component of the unit vector \hat{u}_i . $\mathcal{T}(f, \hat{u}, \hat{k})$ is the timing transfer function for each arm [67, 68].

The expectation of the cross-correlation between the channels I and J is defined as [69]:

$$\langle \tilde{h}_I(f) \tilde{h}_J^*(f') \rangle = \frac{1}{2} \delta(f - f') \Gamma_{IJ}(f) S_h(f), \quad (8)$$

where $S_h(f)$ is the one-sided power spectrum density (PSD) for SGWB, and the overlap reduction function (ORF) [70] for I and J is:

$$\Gamma_{IJ}(f) = \frac{1}{8\pi} \sum_{P=+, \times} \int_{S^2} d\Omega_{\hat{k}} F_I^P(f, \hat{k}) F_J^{P*}(f, \hat{k}) e^{-i2\pi f \hat{k} \cdot \Delta \vec{x}/c}, \quad (9)$$

where $\Delta \vec{x} = \vec{x}_I - \vec{x}_J$, and we define $\vec{x}_{I,J}$ as the location where the interference happens.¹ The ORF reflects the correlation of response between channels I and J , considering a plane wave of frequency f and unit wave vector \hat{k} . When applying to the same channel, *i.e.*, $I = J$, the ORF reduces back to the transfer function.

Combining Eq. (1)–Eq. (5) and Eq. (8), the relation between $\Omega_{\text{gw}}(f)$ and $S_h(f)$ can be derived as [71]:

$$\Omega_{\text{gw}}(f) = \frac{2\pi^2}{3H_0^2} f^3 S_h(f). \quad (10)$$

¹ For a Michelson interferometer, one can understand it as the beam splitter. Although in reality one has to take the time delay interferometry into account which would complicate the idea, the correction is minute which we simply ignore in this study.

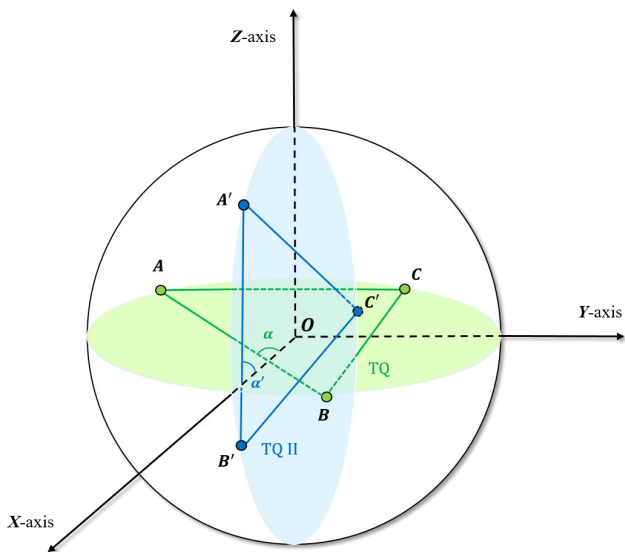


FIG. 1. An illustration of TianQin (green) and TianQin II (blue). α and $\alpha' = \alpha + \beta$ are the initial angles of the two constellations.

B. Detectors and detector networks

The nominal working mode for TianQin is set to “three months on + three months off”: after every three months of the observation, the detector will be down for the next three months [72]. In Fig. 1, we illustrate the detector coordinate system, where the Earth is placed at the origin. The three satellites A, B and C (on the vertices) of the TianQin run on the X-Y plane, we choose the arm length $L_{\text{TQ}} = \sqrt{3} \times 10^5$ km, the displacement measurement noise $S_x^{1/2} = 1 \times 10^{-12}$ m/Hz $^{1/2}$ and the residual acceleration noise $S_a^{1/2} = 1 \times 10^{-15}$ m s $^{-2}$ /Hz $^{1/2}$, as are also listed in Tab. I. Conventionally, the noise level of a GW detector can be represented by its one-sided PSD $P_n(f)$ or the amplitude spectrum density (ASD) $\sqrt{P_n(f)}$ [73]. The ASD of TianQin [35, 74] is shown in Fig. 3. For the Michelson channel, the ASD approaches a constant value beyond $f \simeq 10^{-2}$ Hz, while the A(E) channels oscillate in a sinusoidal way. The Michelson and A/E channel PSD for TianQin can be expressed respectively as:

$$P_{\text{nm}}(f) = \frac{1}{L_{\text{TQ}}^2} \left[S_x(f) + 2 \left(\cos f_c^{\text{TQ}} + 1 \right) \times \frac{S_a(f)}{(2\pi f)^4} \left(1 + \frac{10^{-4} \text{Hz}}{f} \right) \right], \quad (11)$$

$$P_{\text{na,e}}(f) = \frac{1}{L_{\text{TQ}}^2} \frac{4}{3} \sin^2 f_c^{\text{TQ}} \left[\left(\cos f_c^{\text{TQ}} + 2 \right) S_x(f) + 2 \left(\cos(2f_c^{\text{TQ}}) + 2 \cos f_c^{\text{TQ}} + 3 \right) \frac{S_a(f)}{(2\pi f)^4} \left(1 + \frac{10^{-4} \text{Hz}}{f} \right) \right]. \quad (12)$$

TABLE I. Basic parameters of TianQin[35] and LISA[74], where we list the arm length L , the displacement measurement noise $S_x^{1/2}$ and the Residual acceleration noise $S_a^{1/2}$.

Parameter	TianQin	LISA
L	$\sqrt{3} \times 10^5$ km	2.5×10^6 km
$S_x^{1/2}$	1×10^{-12} m/Hz $^{1/2}$	1.5×10^{-11} m/Hz $^{1/2}$
$S_a^{1/2}$	1×10^{-15} m s $^{-2}$ /Hz $^{1/2}$	3×10^{-15} m s $^{-2}$ /Hz $^{1/2}$

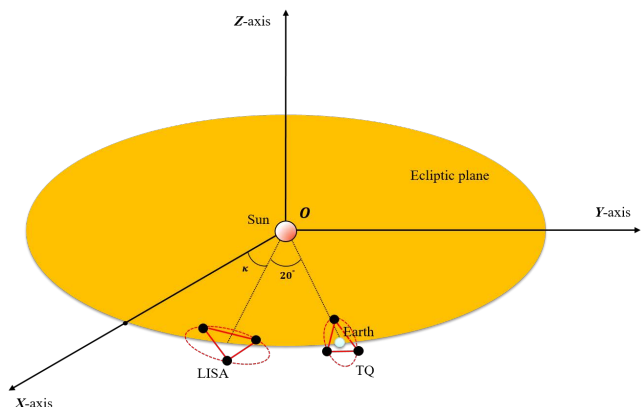


FIG. 2. With the Earth’s revolution around the Sun, the satellites of TianQin circuted around the Earth. On the other hand, LISA revolves around the Sun with $\sim 20^\circ$ in front of the Earth.

Where $f_c^{\text{TQ}} = (2\pi f L_{\text{TQ}})/c$.

In addition to individual detectors, we also consider a network of detectors. We start our discussion with TianQin I+II. The nominal working schedule for TianQin II is to achieve relay of observation and fill in the gaps of TianQin [8, 9]. In Fig. 1, TianQin II is also composed with three satellites (A', B' and C') orbiting around the Earth, of which the orbital plane is perpendicular to TianQin’s. In addition, we also consider the network of TianQin + LISA. In Fig. 2, we illustrate the orbits of TianQin and the LISA in the ecliptic coordinate system. The solar system baryo (SSB) center is located at the center of coordinate system and the ecliptic plane is chosen as the X-Y plane in which both TianQin and LISA revolve around the Sun at the same rate that the Earth moves, keeping a fixed separation of $\sim 20^\circ$ in the orbit of the Earth. The corresponding parameters of LISA is also listed in Tab. I, as well as the ASD of LISA is shown in 3. As a shorthand notation, in figures and equations, we may use TQ for TianQin, TQ II for TianQin II, TT for TianQin I+II, TL for TianQin + LISA, TTL for TianQin I+II + LISA.

III. METHODOLOGY

The output $s(t)$ of each channel in a detector generally consists of the channel noise $n(t)$ and the signal response $h(t)$ on the channel from SGWB [75]. The key

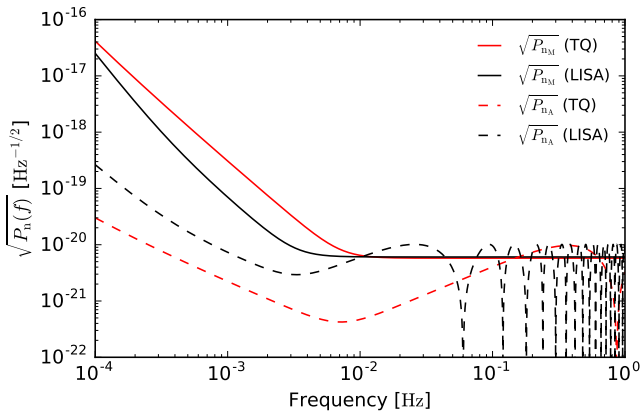


FIG. 3. The ASD $\sqrt{P_n(f)}$ for different channels. The solid and dashed lines denote the Michelson and A(E) channels respectively, where we adopt the red/black to label the TianQin/LISA.

point to the SGWB detection is to distinguish the signal from the noise. Since the SGWB has no waveform template, and unlike the foreground, the signal $h(t)$ of SGWB is generally much weaker than the channel noise, it is hardly possible to employ the excess power statistic from the output to obtain the signal response mentioned in [76], detecting the SGWB within only one channel is difficult [77–88]. However, once a feasible strategies are adopted, the SGWB can be detectable even when the signal is weaker than the noise. Such strategies include performing a correlation between two (or more) independent channels (called the “cross-correlation” [52, 53, 63, 89–92]) and constructing the null channel [55, 56] in a single detector. We shall discuss these two methods in detail and present the formula of the signal-to-noise ratio (SNR) in parallel.

A. The cross-correlation method

The cross correlation method for SGWB detection requires at least two noise-independent channels [93]. Although a single triangle shaped detector contains multiple noise-independent channels, the two channels are also independent for signal [54, 94]. Therefore, one cannot use one triangle-shaped GW detector to detect SGWB through the cross-correlation method.

To perform a cross correlation, one needs to adopt two channels s_I and s_J , in which the only related item are the signals [95]:

$$\begin{aligned} s_I(t) &= n_I(t) + h_I(t) \\ s_J(t) &= n_J(t) + h_J(t). \end{aligned} \quad (13)$$

Here $n(t)$ represents the channel noise and $h(t)$ stands for the GW signal. The noise-independence condition

implies that $\langle n_I(t)n_J(t) \rangle = 0$. If the noises are stationary, we have [96]

$$\begin{aligned} \langle \tilde{n}_I(f)\tilde{n}_I^*(f') \rangle &= \frac{1}{2}\delta(f-f')P_{n_I}(f) \\ \langle \tilde{n}_J(f)\tilde{n}_J^*(f') \rangle &= \frac{1}{2}\delta(f-f')P_{n_J}(f), \end{aligned} \quad (14)$$

where $P_{n_{I,J}}(f)$ is the PSD for the noise of the channels I and J .

Since the noise and the SGWB signal are statistically independent of each other, the expectation value of the cross correlation for two channel outputs is entirely contributed by the SGWB signal:

$$\begin{aligned} \langle S_{IJ} \rangle &\equiv \int_{-T/2}^{T/2} dt \int_{-\infty}^{\infty} df \int_{-\infty}^{\infty} df' \langle \tilde{h}_I(f)\tilde{h}_J^*(f') \rangle \\ &\times \frac{\Gamma_{IJ}(|f|)S_h(|f|)}{P_{n_I}(|f|)P_{n_J}(|f|)} e^{-i2\pi(f-f')t}, \end{aligned} \quad (15)$$

where $S_h(f)$ is defined in Eq. (8) and related to the energy spectrum density of the SGWB via Eq. (10).

Under the assumption that the intrinsic noises of the detectors are significantly larger in magnitude than the SGWB signal: $|n_{I,J}(t)| \gg |h_{I,J}(t)|$, the noise component can be estimated by the variance of the correlation $\sigma^2 \equiv \langle S_{IJ}^2 \rangle - \langle S_{IJ} \rangle^2$. As a result, the expected SNR of the correlated SGWB signals from cross correlating two detectors is given by [97]

$$\text{SNR} \equiv \frac{\langle S_{IJ} \rangle}{\sigma} = \sqrt{2T_{\text{tot}} \int_{f_{\text{min}}}^{f_{\text{max}}} df \frac{\Gamma_{IJ}^2(f)S_h^2(f)}{P_{n_I}(f)P_{n_J}(f)}}} \quad (16)$$

where f_{min} and f_{max} denote the minimum and maximum observation frequency of the channels. The prefactor T_{tot} is the period that two detectors coincidentally operate and its presence suggests that the SNR can be accumulated by means of increasing the coincident operation of two channels.

1. TianQin I+II

We first consider the TianQin I+II when adopting the cross-correlation method. The nominal working mode implies that the two TianQin have no common operation time, which makes the cross correlation inapplicable. Therefore, the aim of detecting SGWB with TianQin I+II requires an extension of the current nominal operation time and puts challenge to the satellite design.

Without loss of generality, suppose at time t , the unit vectors for the three arms of TianQin are constructed in Fig. 1:

$$\begin{aligned} \text{AB} : \hat{u}_1(\alpha) &= (\cos \alpha(t), \sin \alpha(t), 0) \\ \text{AC} : \hat{u}_2(\alpha) &= (\cos(\alpha(t) + \pi/3), \sin(\alpha(t) + \pi/3), 0) \\ \text{BC} : \hat{u}_3(\alpha) &= (\cos(\alpha(t) + 2\pi/3), \sin(\alpha(t) + 2\pi/3), 0), \end{aligned} \quad (17)$$

and those for TianQin II

$$\begin{aligned}
A'B' : \hat{u}'_1(\alpha') &= (\cos \alpha'(t), 0, \sin \alpha'(t)) \\
A'C' : \hat{u}'_2(\alpha') &= (\cos(\alpha'(t) + \pi/3), 0, \sin(\alpha'(t) + \pi/3)) \\
B'C' : \hat{u}'_3(\alpha') &= (\cos(\alpha'(t) + 2\pi/3), 0, \sin(\alpha'(t) + 2\pi/3)).
\end{aligned} \tag{18}$$

Since the noises of TianQin and TianQin II are independent, there are multiple ways to construct two channels for cross-correlation. For a start, we focus on the study of two Michelson channels. Each Michelson channel can be constructed by connecting two adjoint links (following the standard construction) or by a combination of six links. In Fig. 1, a Michelson channel can be built by connecting the links AB and AC of TianQin as well as the other produced by the links A'B' and A'C' of TianQin II. The response functions in these two Michelson channels are:

$$\begin{aligned}
\text{TQ} : F_{M1}^P(f, \hat{k}, \alpha) &= e_{ab}^P(\hat{k}) F_M^{ab}(\hat{u}_1, \hat{u}_2, \hat{k}, f) \\
\text{TQII} : F_{M2}^P(f, \hat{k}, \alpha, \gamma_0) &= e_{ab}^P(\hat{k}) F_M^{ab}(\hat{u}'_1, \hat{u}'_2, \hat{k}, f)
\end{aligned} \tag{19}$$

where the explicit form of F_M^{ab} is defined in Eq. (7). Substituting Eq. (19) into Eq. (9), the ORF for two Michelson channels from TianQin and TianQin II respectively can be written as:

$$\begin{aligned}
\Gamma_{MM}^{\text{TT}}(f, \alpha, \gamma_0) &= \frac{1}{8\pi} \sum_{P=+, \times} \int_{S^2} d\Omega_{\hat{k}} F_{M1}^P(f, \hat{k}, \alpha) \\
&\quad \times F_{M2}^{P*}(f, \hat{k}, \alpha, \gamma_0) e^{-i2\pi f \hat{k} \cdot \Delta \vec{x}_{\text{TQ}}/c}, \tag{20}
\end{aligned}$$

where $\Delta \vec{x}_{\text{TQ}} = A^T A = \frac{L}{\sqrt{3}}(\hat{u}_3(\alpha) - \hat{u}'_3(\alpha, \gamma_0))$, and $\gamma_0(t) \equiv \alpha'(t) - \alpha(t)$.

The instantaneous ORF is dependent on the initial angles α and γ_0 . We can define an averaged effective ORF to that is free of the angle dependence.

$$\hat{\Gamma}_{MM}^{\text{TT}}(f, \gamma_0) = \frac{1}{2\pi} \sqrt{\int_0^{2\pi} d\alpha \left[\Gamma_{MM}^{\text{TT}}(f, \alpha, \gamma_0) \right]^2}. \tag{21}$$

From Fig. 4, one can see that the effective ORF also changes periodically with γ_0 . When $f \gtrsim f_*^{\text{TT}} = \min[c/(2\pi|\Delta \vec{x}_{\text{TQ}}|), c/(2\pi L_{\text{TQ}})] \simeq 0.28$ Hz, $\hat{\Gamma}_{MM}^{\text{TT}}$ is weakly dependent on γ_0 . In contrast, $\hat{\Gamma}_{MM}^{\text{TT}}$ fluctuates substantially and the maxima are localized at fixed value of 0.28. For instance, in the frequency band $f \simeq 10^{-3} - 10^{-1}$ Hz, the effective ORF reaches the optimal performance at $\gamma_0 = n\pi/2, n = 0, 1, 2, 3, \dots$:

$$\Gamma_{MM}^{\text{TT}}(f) = \hat{\Gamma}_{MM}^{\text{TT}}(f, \gamma_0)|_{\gamma_0=n\pi/2}. \tag{22}$$

This suggests that if we aim to optimize the SGWB detection capability, TianQin and TianQin II should be launched in a way that their initial phases differ by the degree $\gamma_0 = n\pi/2$, which set the constraints for the design of the TianQin I+II: the interval that TianQin II enters the orbit should be $n\tau/4$ after that of TianQin,

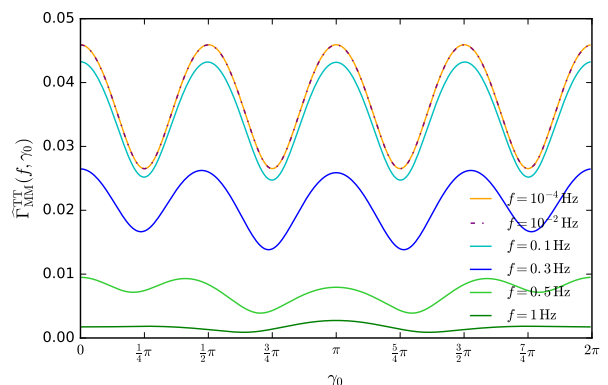


FIG. 4. The dependence of $\hat{\Gamma}_{MM}^{\text{TT}}(f, \gamma_0)$ on γ_0 . The optimal ORF of the TianQin I+II can be obtained after adopting $\gamma = n\pi/2$, where the ORF beyond f_*^{TT} is too weak too to be considered.

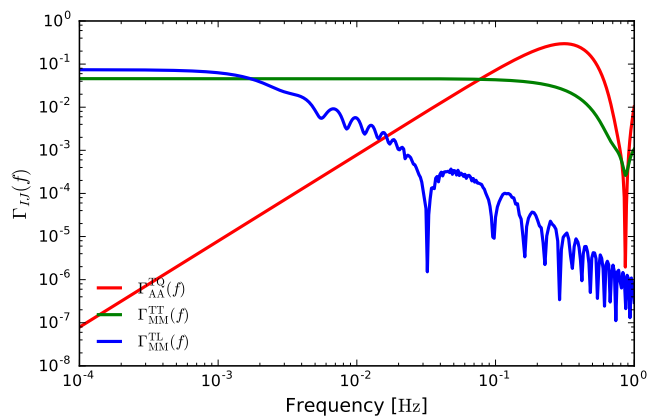


FIG. 5. The response function or ORF for different construction: (i) The red line describes null channel for TDI channels (AE) of TianQin. (ii) The green line is the ORF of TianQin I and II, for which we use Michelson channel and cross-correlation method. (iii) The blue line represents the situation when we combine the Michelson channels of TianQin and LISA by adopting cross-correlation.

with τ being the orbital period for TianQin. We assume the optimal ORF in the preceding analysis. The optimal ORF for present configuration $\Gamma_{MM}^{\text{TT}}(f)$ is shown in the green line in Fig. 5, where the optimal ORF is nearly a constant of 0.046 when $f \ll f_*^{\text{TT}}$.

2. TianQin + LISA

We then extend the study to a network of TianQin + LISA, the configuration is also shown in Fig. 2. According to the time-line of two projects, their operations are scheduled roughly around the same time, with LISA working continuously. This makes it possible to accu-

mulate the relatively long period that TianQin and the LISA runs coincidentally and to perform the joint analysis for the data simultaneously collected. The position vector of the n -th ($n = 1, 2, 3$) TianQin satellites can be decomposed into two parts:

$$\vec{x}_n(t) = \vec{X}(t) + \vec{x}'_n(t), \quad (23)$$

where $\vec{X}(t)$ represents the position of Earth and $\vec{x}'_n(t)$ accounts for the motion around Earth. The components of the $\vec{x}_n(t)$ and $\vec{x}'_n(t)$ in a common coordinate system for TianQin and the LISA are given in the Appendix A and their full expressions can be found in [98] and [99] respectively.

The unit vector for the three arms of the TianQin and the LISA,

$$\begin{aligned} \hat{u}_n(t) &= \epsilon_{nml}(\vec{x}_m(t) - \vec{x}_l(t))/L_{\text{TQ}} \\ \hat{v}_n(t) &= \epsilon_{nml}(\vec{x}'_m(t) - \vec{x}'_l(t))/L_{\text{LISA}}, \end{aligned} \quad (24)$$

the response function for two Michelson channels in the TianQin and LISA are respectively.

$$\begin{aligned} \text{TQ: } F_{M_1}^P(f, \hat{k}, t) &= e_{ab}^P(\hat{k}) F_M^{ab}(\hat{u}_1(t), \hat{u}_2(t), \hat{k}, f) \\ \text{LISA: } F_{M_2}^P(f, \hat{k}, t) &= e_{ab}^P(\hat{k}) F_M^{ab}(\hat{v}_1(t), \hat{v}_2(t), \hat{k}, f). \end{aligned} \quad (25)$$

The ORF of the TianQin-LISA joint network is

$$\begin{aligned} \Gamma_{\text{MM}}^{\text{TL}}(f, t) &= \frac{1}{8\pi} \sum_{P=+, \times} \int_{S^2} d\Omega_{\hat{k}} F_{M_1}^P(f, \hat{k}, t) \\ &\times F_{M_2}^{P*}(f, \hat{k}, t) e^{-i2\pi f \hat{k} \cdot \Delta \vec{x}_{\text{TL}}/c}. \end{aligned} \quad (26)$$

Although the position vectors for the TianQin satellites $\vec{x}_n(t)$ and for the LISA $\vec{x}'_n(t)$ involve the time-dependent angle ($\alpha_{\text{TQ}}(t)$ and $\alpha_{\text{LISA}}(t)$), they are periodic, which leads to a periodic behavior on $F_{M_1}^P$ and $F_{M_2}^P$ as well as $\Delta \vec{x}_{\text{TL}}$. Therefore, the ORF oscillates periodically and the overall performance within one period can be obtained by taking a time average,

$$\Gamma_{\text{MM}}^{\text{TL}}(f) = \frac{1}{\tau} \sqrt{\int_0^\tau dt [\Gamma_{\text{MM}}^{\text{TL}}(f, t)]^2}, \quad (27)$$

where τ is the revolution period of the Earth orbit. We show in blue line in Fig. 5 the averaged ORF for the TianQin-LISA network $\Gamma_{\text{M}}^{\text{TL}}(f)$. Similar to TianQin I+II, the averaged ORF of TianQin + LISA is also a constant of 0.074 as $f \ll f_*^{\text{TL}} = \min[c/(2\pi|\Delta \vec{x}_{\text{TL}}|), c/(2\pi L_{\text{TQ}}), c/(2\pi L_{\text{LISA}})] \simeq 1$ mHz, where we have adopted a LISA arm length of $L_{\text{LISA}} = 2.5 \times 10^6$ km [6].

Before we move on, we highlight the comparison of our results with Seto et al. [87], where the ORF for TianQin I+II and TianQin + LISA are also calculated and presented. There are slight difference in the chose parameterizations: 1. Seto et al. chose the normalised ORF, which differs from our un-normalised ORF by a prefactor

of 5. 2. An interferometer with 60° is equivalent to an L-shaped interferometer with arm length shortened by $\sin(60^\circ)$ [94], this factor is included in our presentation, but is not in Seto et al. 3. Our presentation shows the correlation between a pair of Michelson channels, while Seto et al. includes all pairs, which roughly differs by a factor of 4. Under the long wavelength approximation required by Seto et al., we confirm that we can accurately reproduce results from [87], and our results are consistent to numerical error, while our results does not rely on the long wavelength approximation so still hold valid in higher frequencies.

B. The null channel method

An alternative method is null channel, which is applicable to the SGWB detection at a single TianQin or LISA [54, 100–103]. The key point is to construct three orthogonal channels where the SGWB signal in one of the channels is highly suppressed. The T channel constructed through TDI methods can do just that, with the A/E channels being the signal-sensitive channels. The outputs of the TDI channels can be written as [55]:

$$\begin{aligned} s_{\text{T}}(t) &\simeq n_{\text{T}}(t), \quad f \lesssim f_* \\ s_{\text{A,E}}(t) &= n_{\text{A,E}}(t) + h_{\text{A,E}}(t). \end{aligned} \quad (28)$$

To extract the SGWB signal from the channel noise, the TDI channels should be processed to form a new output:

$$s_{\text{null}}(t) = \sum_{I=\text{A,E}} \left[s_I(t) - \sqrt{\mathcal{Z}_I(t)} s_{\text{T}}(t) \right], \quad (29)$$

as well as the autocorrelation of the new outputs

$$\begin{aligned} K &= \sum_{I=\text{A,E}} \int_{-T/2}^{T/2} dt \int_{-\infty}^{\infty} df \int_{-\infty}^{\infty} df' \tilde{s}_{\text{null}}(f) \tilde{s}_{\text{null}}^*(f') \\ &\times \frac{\Gamma_{II}^{\text{TQ}}(|f|) S_{\text{h}}(|f|)}{P_{\text{nI}}^2(|f|)} e^{-i2\pi(f'-f)t}. \end{aligned} \quad (30)$$

Note that $\mathcal{Z}_{\text{A,E}}(t)$ links the noise of A/E and T in the time domain. And once assuming that $P_{\text{nA,E}}(f) = z(f) P_{\text{nT}}(f)$,

$$\sqrt{\mathcal{Z}(t)} s_{\text{T}}(t) = \int_{-\infty}^{\infty} df \sqrt{z(f)} s_{\text{T}}(f) e^{-i2\pi ft}, \quad (31)$$

where the component $z(f)$ will have no influence on the result of the SNR calculation. The precise definition of $\mathcal{Z}_{\text{A,E}}(t)$ requires the accurate modeling of the channel noises and the real-time simulation data, which are beyond the scope of this article.

By the construction in the Eq. (30), the SGWB signal contributes to the ensemble average of $\langle K \rangle$. On the other hand, the variance is $\sigma^2 = \langle K^2 \rangle - \langle K \rangle^2 \simeq \langle K^2 \rangle$, under

the assumption that $h(t) \ll n(t)$. The SNR ρ of the null channel for the SGWB detection is [104]

$$\rho = \frac{\langle K \rangle}{\sigma} \simeq \sqrt{\sum_{I=A,E} T_{\text{tot}} \int_{f_{\text{min}}}^{f_{\text{max}}} df \left(\frac{\Gamma_{II}^{\text{TQ}}(f) S_h(f)}{P_{n_I}(f)} \right)^2}, \quad (32)$$

where T_{tot} is the observation time. It is straightforward to obtain the transfer function $\Gamma_{AA}^{\text{TQ}}(f)$ for TianQin through Eq. (9)². In the ideal symmetric scenario, the PSDs and the transfer functions of A and E channels take the same form [106]. In this case, Eq. (32) reduces to:

$$\rho = \sqrt{2T_{\text{tot}} \int_{f_{\text{min}}}^{f_{\text{max}}} df \left(\frac{\Gamma_{AA}^{\text{TQ}}(f) S_h(f)}{P_{n_A}(f)} \right)^2}, \quad (33)$$

The response function Γ_{AA}^{TQ} adopted can be found as the red line in Fig. 5. The A/E channel is constructed as the difference between two Michelson channels delayed in time by $2L/c$, therefore, for frequency $f \rightarrow 0$, *i.e.*, the GW wavelength $\lambda \gg L$, the difference vanishes and one has $\Gamma_{AA}^{\text{TQ}}(f) \rightarrow 0$.

We remark that the general assumption that the background is much weaker than the noise is not universal. When the condition is invalid, it is no longer appropriate to calculate the SNR with the Eq. (16) or Eq. (33). The modified expression for the SNR is [67, 107]:

$$\text{SNR} \equiv \frac{\langle S_{IJ} \rangle}{\sigma} = \sqrt{2T_{\text{tot}} \int_{f_{\text{min}}}^{f_{\text{max}}} df \frac{\Gamma_{IJ}^2(f) S_h^2(f)}{P_{n_I}(f) P_{n_J}(f) W_C(f)}}, \quad (34)$$

where the correction term $W_C(f)$ is:

$$W_C(f) = 1 + \frac{S_h(f) [\Gamma_{II}(f) P_{n_I}(f) + \Gamma_{JJ}(f) P_{n_J}(f)]}{P_{n_I}(f) P_{n_J}(f)} + \frac{[\Gamma_{IJ}(f) S_h(f)]^2 \left[1 + \frac{\Gamma_{II}(f) \Gamma_{JJ}(f)}{\Gamma_{IJ}^2(f)} \right]}{P_{n_I}(f) P_{n_J}(f)}. \quad (35)$$

Notice that this expression is versatile and can extend to the null channel methodology, by setting $I = J$.

From Eq. (16) and Eq. (33), one can conclude that no matter what method is adopted, the SNR for SGWB detection is proportional to $\sqrt{T_{\text{tot}}}$. However, based on the above results, it is not straightforward to determine which configuration is the best for SGWB detection. In the next section, we will assess the SGWB detection capability of different configurations.

C. Power-law integrated sensitivity curve

The relation between the SGWB strength to a detector sensitivity is not straightforward. A convenient

way of illustrating the sensitivity is to assume a power-law spectrum of SGWB $\Omega_{\text{gw}}(f) = \Omega_\epsilon (f/f_{\text{ref}})^\epsilon$ ³ [108], and present the *power-law integrated sensitivity curve*. There's only two free parameters in this expression where reference frequency f_{ref} can be arbitrary, and Ω_ϵ is related to ϵ . One can thus define the PI sensitivity curve $\Omega_{\text{PI}}(f) = \max_\epsilon [\Omega_\epsilon (f/f_{\text{ref}})^\epsilon]$, where the power-law energy density is defined as [109]:

$$\Omega_\epsilon = \rho_0 \left[2T_{\text{tot}} \int_{f_{\text{min}}}^{f_{\text{max}}} df \frac{(f/f_{\text{ref}})^{2\epsilon}}{\Omega_n^2(f)} \right]^{-1/2}, \quad (36)$$

and ϵ is chosen as $-10, -9, \dots, 9, 10$, ρ_0 is the SNR threshold, and the corresponding energy density is defined as

$$\Omega_n(f) = \frac{2\pi^2}{3H_0^2} f^3 \sqrt{\frac{P_{n_I}(f) P_{n_J}(f)}{\Gamma_{IJ}(f)}}, \quad (37)$$

where $I \neq J$ and $I = J$ is related to the cross-correlation and the null channel respectively.

In Fig. 6, we present the PI sensitivity curves under different configurations, assuming an operation time $T_{\text{op}} = 1$ yr. Notice that due to the working mode of TianQin, the nominal observation time for the TianQin-LISA joint network $T_{\text{tot}} = T_{\text{op}}/2$. For TianQin and TianQin II, the nominal design does not contain overlap in observation time, and we have to discuss on basis of a different observation scenario, which we choose to consider a ‘‘four months on + two months off’’ scheme, therefore, one can expect four months of joint observation per year.

In order to make a fair comparison of detection capabilities between different configurations, one has to take several factors into account. From a superficial glance, one might jump into the false conclusion that the single TianQin possesses a better capability for SGWB, especially for frequencies beyond a few mHz. This is only partially true: the most ideal case for detecting an SGWB through cross-correlation method would involve multiple detectors that have maximum correlation in signal and zero correlation in noise, and the maximum correlation in signal is only achieved when the two detectors are co-located and co-oriented. Therefore, for a general multi-detector network, a finite difference in orientation and location between detectors reduces their ability to detect the SGWB. Secondly, a simultaneous operation between multiple detectors is critical for the SGWB detection, and the total simultaneous operation time T_{tot} is always shorter than the single detector operation time. These two factors reduce the sensitivity for the cross-correlation method compared with the null channel method. However, recall that in order for the null channel to succeed, one has to rely heavily on the detailed

² In some studies ([e.g. 105]), the definition of the transfer function can differ our definition by a constant numerical factor.

³ Readers are reminded that this form does not imply an Einstein summation

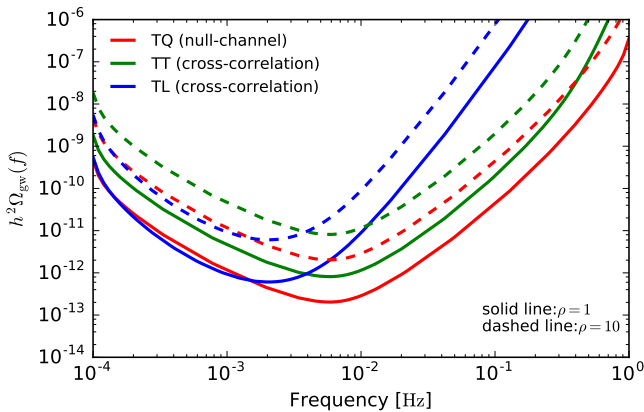


FIG. 6. The PI sensitivity curves for various of detector configurations. The operation time is set to $T_{\text{op}} = 1$ yr and SNR threshold $\rho_0 = 1, 10$. We expect a 0.5 years per year observation time for TianQin and TianQin + LISA; while we assume 4 months per year observation time for TianQin I+II under a modified working schedule, as the nominal operation scheme does not permit joint observation.

understanding of the detector noises, while the cross-correlation represents a much more feasible approach. Therefore, conceptually, the cross-correlation method is much more robust and reliable than the null channel method.

Finally, we remark that there are multiple methods of presenting SGWB sensitivity. In addition to the PI curve we adopt in this work, some might adopt a peak-integrated sensitivity curve (PISC) that assumes a peak-shaped form of SGWB spectrum [110], in which case the maximization process adopted in PI sensitivity curve can be omitted. Notice also for the PI curve to gain the benefit of assessing SNR in a straightforward way, the strength of SGWB is fixed, while sensitivity curve becomes inversely proportional to observation time [45, 111, 112]. On the other hand, some literatures prefer to present the SGWB in a time-independent and threshold-independent style through the corresponding energy density Ω_n [24, 113–115].

IV. THE SPECTRUM OF SGWB

In this section, we briefly review a number of the potential sources for the SGWB in the mHz range. The sources can be divided into two classes, namely, astrophysical SGWB and the cosmological SGWB, and we study their strength as well as spectral shape. The former contains inspirals of the DWDs, binary neutron stars (BNSs), and SBBHs [63, 116–121]. The latter can be raised by a number of physical process: like the quantum fluctuation during inflation [122], the decay of the false vacuum [123] and the evolution of the cosmic string [124]. Note that we discuss different sources separately, and we leave the

problem of distinguishing SGWB of different origins for the future discussion.

A. Foreground

There are a great amount of DWDs in our Galaxy, each emitting a quasi-sinusoid GW signal. At certain frequency bins, especially for lower frequencies, there might contain a number of DWDs emitting GWs with similar amplitudes. Due to the vast majority of these DWDs, the sheer amount of these signals cause them to overlap each other, making the identification of any single signal, except for the very strong ones, essentially impossible. The signals would then form a foreground by incoherent superposition [27, 125–127].

In order to derive the foreground, we first calculate the frequency-domain signals $\tilde{h}(f)$ for all the DWDs in each frequency bin. The initial estimate for the foreground spectrum can thus be obtained by the sum of squares for $\tilde{h}(f)$ per frequency bin, and the overall spectrum is simply the sum of squares of both the foreground $S_{\text{DWD}}(f)$ and the instrumental noise $S_n(f)$. We remove the fluctuations in this initial estimate, by binning over the frequencies to use median values within as representatives, which are further downsampled to a handful of points. A cubic spline fit is later performed on top of these samples [128], and a smooth estimate of the PSD, consisting of both the foreground caused by the DWDs $S_{\text{DWD}}(f)$ and the instrumental noise $S_n(f)$, is thus obtained. A source is identified as “resolvable” (and later removed from the sample) if the expected SNR exceeds the preset detection threshold of 7 [129]. The aforementioned process is then repeated iteratively, continuously lowering the PSD, until when no new resolvable source is identified.

As the observation time increases, more individual DWDs can exceed the pre-determined threshold of detection. The identification and the later removal of the stronger DWDs will in turn lower the strength of the foreground. A preliminary study reveals that for a nominal observation time of five years, the accumulated foreground of TianQin would be under the ASD [8]. We fit the foreground with an exponential of the polynomial. For the numerical coefficients, we direct interested readers to table II and figure 3 from [8]. We are thus confident that for the individual detection and measurement of the other signals at TianQin, the GW foreground has marginal effects. However, as the foreground has comparable strength of the noise ASD, its existence would still overshadow the SGWBs of other origins.

In the existing literatures within the authors’ reach, all discussions on the GW foreground concentrate on the single GW detector either for the LISA [74], for DECIGO [36], or for TianQin [8]. Notice that [87] discussed the detection prospect of a detector network on SGWB, but the implication of joint detection on foreground is not explicitly discussed. However, notice that the expected

operation time of TianQin and LISA might have a certain amount of overlap, it is meaningful to discuss the implication on GW foreground under a network of the space-borne GW detectors.

For the individually resolvable sources, the optimal SNR is defined as the inner product of the expected waveform $\tilde{h}(f)$

$$\rho_{\text{opt}}^2 \triangleq (h|h) = 4\Re \int_0^\infty df \frac{\tilde{h}(f)\tilde{h}^*(f)}{P_n(f)}, \quad (38)$$

which denotes the optimal capability for the source with the waveform $\tilde{h}(f)$, and \Re is the real part (which can be ignored here since $h(f)h^*(f)$ is guaranteed to be real). Besides, the total SNR with a GW detector network ρ_{tot} is the root sum square of SNRs from each detectors ρ_i [130, 131]

$$\rho_{\text{tot}} = \sqrt{\sum_i \rho_i^2}. \quad (39)$$

Defining the effective PSD P_{ntot} with a network of GW detectors [132]

$$P_{\text{ntot}}(f) = \frac{1}{\sum_i P_{ni}^{-1}(f)}, \quad (40)$$

the total SNR can be obtained through Eq. (38) when an all-sky average on the detector response is assumed, *i.e.*, we assume that after averaging, $\tilde{h}(f)$ is kept unchanged across the different detectors.

$$\begin{aligned} \rho_{\text{tot}}^2 &= \sum_i 4\Re \int_0^\infty df \frac{\tilde{h}(f)\tilde{h}^*(f)}{P_n^i(f)} \\ &= 4 \int_0^\infty df \sum_i \frac{\tilde{h}(f)\tilde{h}^*(f)}{P_n^i(f)} \\ &= 4 \int_0^\infty df \frac{\tilde{h}(f)\tilde{h}^*(f)}{P_{\text{ntot}}(f)}. \end{aligned} \quad (41)$$

Based on the Eq. (39) and Eq. (40), one can estimate the foreground on a detector network by removing the resolvable sources with $\rho_{\text{tot}} \geq 7$. In Fig. 7, we present such foreground with 0.5 years, 1 year, 2 years, and 4 years operation time, respectively, assuming a network of TianQin and the LISA. The joint observation of TianQin and the LISA will increase the sensitivity by reducing the effective PSD, as a result, more sources are expected to be recovered compared with a single constellation, which in return pushes the joint foreground downwards. From Fig. 7 we can easily deduce that the network foreground will be constantly below the PSD of TianQin. Moreover, in Fig. 8, we also compare the expected number of the resolvable DWDs under the different detector/network and the operation time. Notice that compared with the union of samples from an individual constellation, a network of TianQin and the LISA could boost the number of the resolvable sources by about 5% ~ 12%, and the number can be further increased to around 8% ~ 22% if TianQin II is included, as shown in Fig. 8.

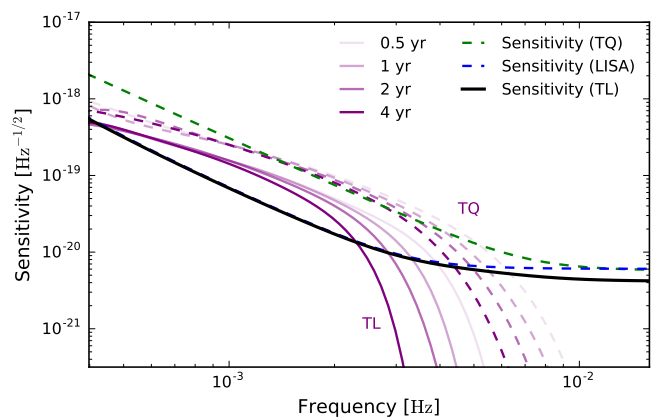


FIG. 7. The dashed green curve represents the ASD of TianQin, and the dashed blue curve represents the ASD of LISA. The black solid line is the effective ASD for the joint network of TianQin and LISA. The foreground for the TianQin (dashed line) and TianQin-LISA network (solid line) are shown with different shades of purple, assuming a 0.5 years, 1 year, 2 years, and 4 years operation time, respectively. Note that observation/off repetitive pattern for TianQin has been accounted for in the calculation.

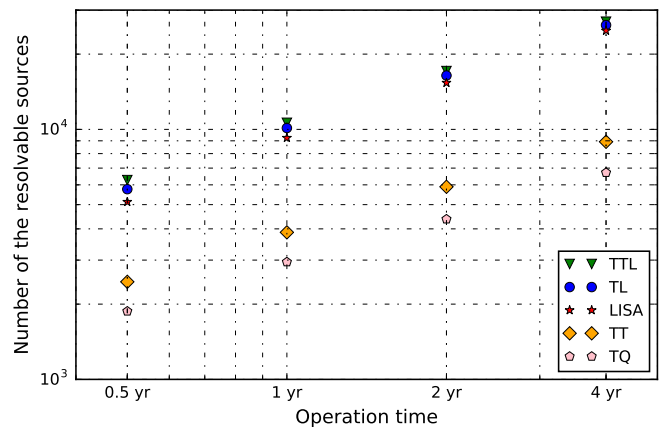


FIG. 8. The number of resolvable DWDs under different detector/network. Red star, blue dot and green triangle represent the union of sources from individual detectors, TianQin-LISA network and a network of TianQin I+II and LISA, respectively.

B. SGWB from compact binary objects

Astrophysical sources other than the DWDs are not expected to be strong enough to reach the level of the noise PSD, but the formed SGWB can still be detectable.

Compact binary coalescences like mergers of SBBHs as well as BNSs have been identified by ground-based GW detectors [133–137]. Such compact binaries can emit the mHz GW signals during the early inspiral stage months to years prior to the merger, which can be detected by

TABLE II. The SNRs for the SGWBs from SBBH and BNS, assuming one year operation time.

	SBBH	BNS
TQ (null channel)	$3.26_{-1.17}^{+2.03}$	$0.89_{-0.67}^{+1.36}$
TQ I+II (cross-correlation)	$0.81_{-0.29}^{+0.51}$	$0.22_{-0.17}^{+0.34}$
TQ+LISA (cross-correlation)	$0.55_{-0.20}^{+0.34}$	$0.15_{-0.11}^{+0.23}$

the space-borne GW detectors [138?, 139]. It's expected that such signals can stack up to form a SGWB.

With a k -th type of the compact binaries described by the population properties θ_k (like the component masses, spin, orbital eccentricity, and progenitor metallicity, *etc.*), following [140, 141], the spectrum density of SGWB $\Omega_{\text{gw}}(f)$ from each component can be formulated as the superposition of each binary's energy spectrum:

$$\Omega_{\text{gw},0}(f) = \frac{f}{\rho_c} \int d\theta_k \int_0^{z_{\text{max}}} dz \frac{R_m(z, \theta_k) \frac{dE_{\text{gw}}}{df_s}(f_s, \theta_k)}{(1+z)H(z)}, \quad (42)$$

where $R_m(z, \theta_k)$ is the merger rate, and $\frac{dE_{\text{gw}}}{df_s}$ profiles the energy spectrum emitted in the source frame $f_s = f(1+z)$. $H(z)$ is the Hubble parameter, by making the maximum redshift $z_{\text{max}} = 10$ (above which not many astrophysical black holes are expected to be formed due to the lack of star formation), $H(z)$ can be safely approximated as $H_0 \sqrt{\Omega_m(1+z)^3 + \Omega_\Lambda}$ [59]. In this work, we do not consider the influence of the orbital eccentricity for the binaries. Furthermore, instead of the evolving merger rate density model [17, 142–144], we adopt the official merger rate derived from the observation of the ground-based detectors, in which the redshift evolution is also not included [145], *i.e.*, $R_m(z, \theta_k)$ is independent of the redshift. For the mass distribution, we adopt the “POWER LAW + PEAK” model in [145] for the stellar mass SBBHs, which is equivalent to “Model C” described in [146], where $5M_\odot \leq m_2 \leq m_1 \leq 100M_\odot$. As for the BNSs, we adopt a uniform component-mass distribution [147] ranging from $1M_\odot - 2.5M_\odot$ without redshift evolution. We adopt the value $R_m(0, \theta_{\text{BBH}})$ of $23.9_{-8.6}^{+14.9} \text{ Gpc}^{-3} \text{ yr}^{-1}$ and $R_m(0, \theta_{\text{BNS}})$ of $320_{-240}^{+490} \text{ Gpc}^{-3} \text{ yr}^{-1}$ provided by [145] as the merger rate. For the energy spectrum, dE_{gw}/df_s , we adopt the same format as [148], which considers the updated IMR phenomenological waveform [149]. In Tab. II, we list the expected SNRs for SBBH and BNS, considering the above range of merge rate R_m and assuming one year operation time.

The similar procedure is also applied to the MBHBs with masses range between 10^2M_\odot to 10^8M_\odot , to estimate the corresponding SGWB. MBHBs can emit strong GW signals in a wide range of frequency, and the Pulsar Timing Arrays (PTA) is expected to resolve the individual mergers as well as detect the SGWB in the nHz band [150–152]. Space-borne GW detectors oper-

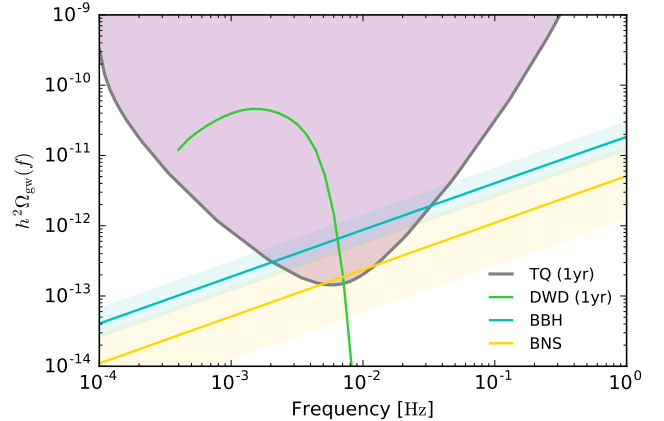


FIG. 9. The spectrum density $\Omega_{\text{gw}}(f)$ of the DWDs (green), the SBBHs (blue), the BNSs (orange) are shown together with the PI sensitivity curve (gray) for TianQin with 1 yr operation time. The foreground produced by the DWDs dominates in the mHz band, where the backgrounds produced by the SBBHs and the BNSs are expected to be submerged.

ate in the mHz band can observe the individual mergers [9, 153], but the corresponding SGWB is unlikely to be detectable [154–156]. Based on the astrophysical models for MBHB mergers adopted by [9], we conclude that the SGWB is indeed too weak to be detectable by TianQin.

We also considered sources with other origins, like the core-collapse supernovae [157, 158], rotating neutron stars [159, 160], and magnetars [161, 162]. The spectrum are studied and we conclude that their strengths are not strong enough to be detectable by TianQin.

C. SGWB from inflation

In addition to the astrophysical origin, the amplification of the quantum tensor fluctuations of the spacetime experienced during inflation and rapidly stretched to beyond the horizon produces the primordial GWs, which turns into a relic stochastic background of the GWs when re-entering the horizon after inflation [163–166]. This constitutes an irreducible source of the GWs that are expected from any inflationary model [167]. For the tensor modes with the frequencies of few mHz, they re-entered the horizon in the deep radiation-dominated era. The propagation of this primordial background until the present leads to the GW energy density spectrum today [168]:

$$h_0^2 \Omega_{\text{gw}}(f) = 0.016 \cdot h_0^2 \Omega_r^0 r \mathcal{P}_{\mathcal{R}} \left(\frac{f}{f_{\text{CMB}}} \right)^{n_T}, f \geq 10^{-4} \text{ Hz}, \quad (43)$$

where the Hubble constant $h_0 = 0.674$ [59], and the radiation energy density today $\Omega_r^0 = h_0^{-2} \cdot 4.17 \times 10^{-5}$ [169],

the primordial curvature power spectrum $\mathcal{P}_{\mathcal{R}} \simeq 2.14 \times 10^{-9}$ associated with the pivot frequency $f_{\text{CMB}} = 7.73 \times 10^{-17}$ Hz [170].

Clearly, the order of $h_0^2 \Omega_{\text{gw}}$ depends on the tilt of the tensor spectrum n_T and the tensor-to-scalar ratio r [171]. For the minimal model where a single scalar field drives a slow-roll inflation, these two parameters obey the consistency relation $n_T = -r/8$. As a result, the prediction for $h_0^2 \Omega_{\text{gw}}$ in the minimal inflation model is entirely determined by the size of r . The most stringent bound $r \lesssim 0.056$ from the Planck [170] demands a very small $|n_T|$, resulting a nearly scale-invariant power spectrum with $h_0^2 \Omega_{\text{gw}}(f) \lesssim 6 \times 10^{-17}$. It is a value at least 3 orders of magnitude below the TianQin sensitivity curve and the primordial background is thus inaccessible at the TianQin.

Beyond the irreducible emission GW backgrounds with a high amplitude and a significant deviation from scale-invariance, can also be produced if new species or symmetries are introduced during inflation [173–178]. However, the discussion of these inflationary backgrounds is beyond the scope of this paper.

D. SGWB from first order PT

In addition to the primordial GWs formed during the inflationary period, the SGWB can also be generated after inflation where the important sources include the primordial black holes (PBHs) [179, 180], the non-perturbative effects in the reheating epoch [181], the PTs of the early Universe [182] and the cosmic defects [183, 184]. In this section we discuss the last two sources as they have strong relation to the inflationary models and TeV-scale physics.

Generating the SGWB from the first-order PTs [185–188] is a theoretically favorable scenario given the fact that the electroweak symmetry of the elementary particle physics are broken in the present Universe. A first-order PT in the early Universe corresponds to a tunnelling process from a symmetric phase to a broken phase with a lower energy (true vacuum) through the nucleation of bubbles of the true vacuum that receive the vacuum energy released from the PT. Following the nucleation [14] the bubbles expand and eventually collide with others, eventually causing the gravitational radiation due to the destruction of the spherical symmetry preserved in a single vacuum bubble [189]. This physical process has been described by the envelope approximation model [189] that assumes the liberated vacuum energy is entirely concentrated in the bubble wall and neglects the overlapping regions of the colliding bubbles.

The recent successful large-scale hydrodynamical simulation [190] has revealed that, for a PT happening in the thermal cosmic medium, the majority of the vacuum energy stored in the bubble wall does not dissipate after the collision but transfer to the surrounding plasma fluid, which may give rise to a substantial amount of the GW

radiation in the form of sound waves and turbulence due to the movement of the plasma fluid caused by the bubble collision [191]. Nonetheless, as of the current knowledge neither the acoustic production mechanism nor the origin of the vortical turbulence has been yet fully understood. The sound-shell model [192] has attempted to explain the former puzzle. Ignoring the interference between the one source and another, we linearly superimpose these three contributions in computing the total SGWB observed today,

$$h_0^2 \Omega_{\text{gw},0}(f) = \sum_i h_0^2 \Omega_{i,0}(f), \quad (44)$$

where the sum includes the collision occurring during the PT, acoustic and turbulent phases after the PT. The individual contribution after taking into account the red-shift can be written in terms of a compact form,

$$h_0^2 \Omega_{i,0}(f) = 1.67 \times 10^{-5} \left(\frac{100}{g_*(T_*)} \right)^{1/3} S_i(f, \tilde{f}_i) \left(\frac{H_*}{\beta} \right)^p \left(\kappa_i(\alpha) \frac{\alpha}{1+\alpha} \right)^q \tilde{\Delta}_{i*}(v_w), \quad (45)$$

where the indices p, q , the spectral function $S_i(f, \tilde{f}_i)$, the peak amplitude $\tilde{\Delta}_{i*}(v_w)$ and the efficient factor $\kappa_i(\alpha)$ are collected in Tab. III. Similarly, the red-shifted peak frequency today for each source takes the form [193],

$$\tilde{f}_i = 1.65 \times 10^{-5} \text{ Hz} \frac{\tilde{f}_{i*}}{\beta} \left(\frac{\beta}{H_*} \right) \left(\frac{T_*}{100 \text{ GeV}} \right) \left(\frac{g_*(T_*)}{100} \right)^{\frac{1}{6}}, \quad (46)$$

with the peak frequency before the redshift \tilde{f}_{i*} given in Tab. III.

Two important remarks on the peak parameters are placed in order. First, the state-of-art development introduces the sound shell thickness $L_S = R_*(1 - c_s/v_w)$ [194] in addition to the mean bubble separation $R_* = (8\pi)^{1/3} v_w/\beta$ [195], with $c_s = 1/\sqrt{3}$ being the the sound speed. This modification respects the new observation that the length scale of the acoustic waves is characterized by the thickness of the sound shell and will cause a red-shift on the peak frequency of the GW power spectrum as the bubble velocity v_w decreases. The other improvement made in [172] involves an accurate estimate on the duration of the acoustic production,

$$\tau_{\text{sw}} = \min [H_*^{-1}, R_*/U_f], \quad (47)$$

where U_f is the average square root of fluid velocity [196]. This treatment is particularly crucial for the strong PT where the fluid develops into the turbulence within one Hubble time [197], otherwise the contribution from the turbulent phase would be underestimated.

From Eq. (45) it is apparent that the red-shifted SGWB spectrum generated from the PT is entirely determined by the properties of the PT including the PT

TABLE III. The ingredients of the GW spectra from the PT, where α_∞ determines the weakest transition above which a portion of the vacuum energy converts into the kinetic energy driving the bubble expansion [172]. The Hubble parameter at the moment of GW production with the total number of relativistic degrees of freedom g_* and the temperature T_* at the time when GWs are produced: $h_* = 1.65 \times 10^{-5} \text{ Hz} \left(\frac{T_*}{100 \text{ GeV}} \right) \left(\frac{g_*}{100 \text{ GeV}} \right)^{1/6}$.

i	p	q	$\tilde{\Delta}_{i*}(v_w)$	$\frac{\tilde{f}_{i*}}{\beta}$	$S_i(f, \tilde{f}_i)$	$\kappa_i(\alpha)$
col	2	2	$\frac{0.44v_w^3}{1+8.28v_w^3}$	$\frac{0.31}{1-0.051v_w+0.88v_w^2}$	$\frac{3.8(f/\tilde{f}_i)^{2.9}}{1+2.9(f/\tilde{f}_i)^{3.8}}$	$\max[1 - \frac{\alpha_\infty}{\alpha}, 0]$
sw	1	2	$0.157v_w H_* \tau_{\text{sw}}$	$1.16 \frac{L_s}{R_*}$	$\left(\frac{f}{\tilde{f}_i}\right)^3 \left(\frac{7}{4+3(f/\tilde{f}_i)^2}\right)^{7/2}$	$\begin{cases} \kappa(\alpha_N) _{\alpha_N=\alpha}, \alpha \leq \alpha_\infty \\ \frac{\alpha_\infty}{\alpha} \kappa(\alpha_N) _{\alpha_N=\alpha_\infty}, \alpha > \alpha_\infty \end{cases}$
turb	1	$\frac{3}{2}$	$20v_w(1 - H_* \tau_{\text{sw}})$	$1.33 \frac{L_s}{R_*}$	$\frac{(f/\tilde{f}_i)^3}{[1+(f/\tilde{f}_i)]^{\frac{11}{3}}(1+8\pi f/h_*)}$	

TABLE IV. The SNRs for the SGWB from PT, where the parameters are fixed to $\alpha = 0.5, v_w = 0.95, T_* = 100 \text{ GeV}$, and set $\beta/H_* = 10, 100, 1000$, and assuming one year operation time.

	$\beta/H_* = 10$	$\beta/H_* = 100$	$\beta/H_* = 1000$
TQ (null channel)	11	220	240
TQ I+II (cross-correlation)	2.8	60	61
TQ+LISA (cross-correlation)	14	72	11

scale T_* , the PT strength α and the PT duration (normalized to the Hubble parameter) β/H . As an example, we consider a PT occurring at the electroweak scale $T_* = 100 \text{ GeV}$ with a moderate strength $\alpha = 0.5 \leq \alpha_\infty$ and the short duration $\beta/H = 10, 100, 1000$ and adopt a quantitative estimate that was performed in [194]. The produced red-shifted SGWB spectrum shown in Fig. 10 is typically peaked within the frequency band of $\mathcal{O}(10^{-4} - 10^{-1}) \text{ Hz}$, where the space-borne GW detectors (including TianQin) reach the best sensitivity. This could lead to a substantially larger SNR for the GW signal that could be detected. The corresponding SNRs are shown in Tab. IV.

In addition to a single-peak spectrum, more exotic shapes of the GW spectrum such as the multi-peak one are also possible [89, 198]. Since the first-order electroweak phase transition (EWPT) is not achievable in the Standard Model (SM) [199, 200], any detection of the GWs from the EWPT would provide a unique probe for the nature of the EWPT triggered by new physics beyond the SM that is difficult to be measured at the colliders.

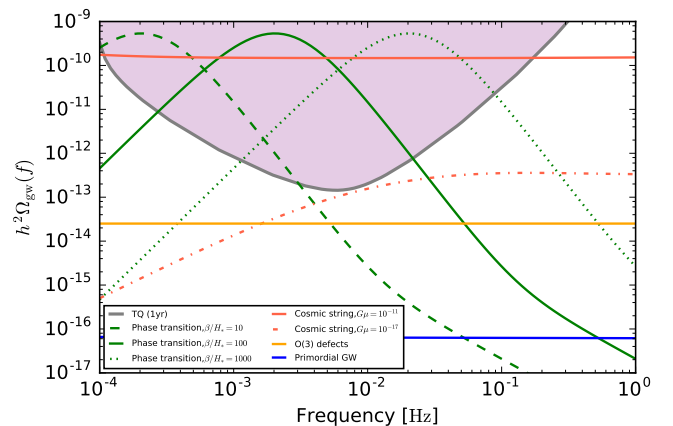


FIG. 10. To obtain green line, we neglect the contribution of scalar field, and set $\alpha = 0.5, v_w = 0.95, \beta/H_* = 10, 100, 1000, T_* = 100 \text{ GeV}$. As for the SGWB produced by inflation, we set the tensor-to-scalar ratio $r = 0.056$ [170]. When calculating the SGWB for cosmic defects, we set $G\mu = 10^{-11}, 10^{-17}$ for string loops decay, and $N = 3, v = 10^{16} \text{ GeV}$ [201] for $O(N)$ theory to obtain the spectrum respectively. Because the model dependent of them are remarkable, We can not determine the exact value but a certain range of the SNR in Tab. VI.

E. SGWB from cosmic defects

The formation of the cosmic defects is another important product of a PT, particularly for the one that happens in the inflationary period or shortly after the inflation. Such formation is closely associated with a (spontaneous) breaking for continuous symmetry and typically arises in the case that the vacuum produced from the PT is topologically non-trivial [202]. Depending on the dimensionality of the defect network, the cosmic defects are divided into topological and non-topological. The topological defects include domain walls, strings and monopoles [203] that will be specifically discussed.

In what follows we first describe the irreducible emission of the GWs from any type of the cosmic defect net-

work. Once formed during the radiation-dominated (RD) era, any defect network always radiate the GWs with an exact scale-invariant energy density spectrum [204]. This remarkable feature of the scale-invariance was first confirmed by the numerical simulation [205]. Nonetheless, the SGWB spectrum produced in the full cosmic history turns out to be no longer scale-invariant in the entire frequency range [206]. This is due to a substantial GW emission from the modes that entered during the matter-dominated (MD) over the one from the RD era below the frequency at the matter-radiation equality. In contrast, this contribution is extremely weak in the TianQin frequency band and thus does not destroy the scale-invariance in the GW spectrum. For simplicity, in the numerical analysis we consider the irreducible background of the GWs produced during the RD era only with its amplitude characterized by the symmetry breaking scale and the nature of the defects.

For the global $O(N)$ theory, the formation of cosmic defects is possible upon the spontaneously breaking into $O(N-1)$ symmetry. Especially, non-topological defects such as the texture arise for the large N limit $N \geq 3$. The SGWB spectrum today corresponding to these sources take a universal form [204, 207]

$$h_0^2 \Omega_{\text{gw},0} \simeq \frac{650}{N} \tilde{f}(N) h_0^2 \Omega_r^0 \left(\frac{v}{M_{\text{Pl}}} \right)^4, \quad (48)$$

where the prefactor $\tilde{f}(N)$ is included to match the numerical result and, to a good approximation, can be parametrized as $\tilde{f}(N) = 1.1 + 45/N^2$ [204]. Therefore, Eq. (48) suggests that the amplitude of this SGWB today is suppressed by N and increases with the factor $(v/M_{\text{Pl}})^4$, with v being the scale of the symmetry breaking and the Planck mass $M_{\text{Pl}} \simeq 1.22 \times 10^{19}$ GeV. We find that the cosmic defects from an $O(3)$ breaking at the scale $v \lesssim 10^{16}$ GeV produce GW signal whose magnitude is roughly one order below the TianQin sensitivity curve. This indicates only the cosmic defects formed close to the Planck scale are detectable at the TianQin.

As a special example, we shall focus on the one-dimensional topological defect: cosmic strings [208, 209]. In general, cosmic strings can be either fundamental (super) strings built in the string theories or stable strings admitted in the field theories [210], *i.e.* the structurally simplest $O(2)$ or $U(1)$ theories [211–213]. For the infinite thin string (Nambu-Goto (NG) string), either type of the strings are typically characterized by a single dimensionless quantity $G\mu$ (with the Newton constant G and the string energy density μ), which is related to the symmetry breaking scale v via $G\mu = \pi(v/M_{\text{Pl}})^2$ [214]. However, these two types of strings have different properties such as the way and the probability when the strings collide [215]. This main difference significantly affects the evolution of the string network, and the production of the GWs expected from the decay of the loops.

The history of the string network from the formation to the present time is described as follows. Once created,

a string network is stretched by the cosmological expansion, and the relativistic motion of the strings leads to string self-intersects or two curved strings collide, forming the loop constantly. Loops smaller than the horizon decouple from the cosmological evolution and oscillate under their own tension, slowly decaying into the GWs, whose spectrum is primarily constituted by bursts from the cusps, kinks and kink-kink collisions⁴.

Other than the sub-horizon loops, the historical remnants of network also contain the super-horizon loops and even open strings, both of which stretch across a Hubble volume. Although these strings also emit the GWs coming from the accumulation of their small-scale structure, for the NG cosmic string networks this background play an insignificant role in the emission of the GW background. Thus, we will not include this contribution in the following analysis of the paper.

The recent simulations of the cosmic string networks [217] favor the large sub-horizon loops with the size $\alpha_l \gg \Gamma G\mu$ produced by the network. In this case, the total SGWB spectrum from the whole network of the loops can be approximately estimated by means of adding the GW emission from all the loops throughout the entire history of the Universe. This includes the contribution of the loops that are created and decay in the RD era, of the RD era loops that decay during the MD era and of the loops created in the MD era.

$$\Omega_{\text{gw}}(f) = \Omega_{\text{gw}}^{\text{r}}(f) + \Omega_{\text{gw}}^{\text{rm}}(f) + \Omega_{\text{gw}}^{\text{m}}(f). \quad (49)$$

Each component takes the common form [215, 218]

$$\Omega_{\text{gw},0}^i(f) = \frac{8\pi(G\mu)^2}{3H_0^2 f} \sum_{k=1}^{\infty} 2k \mathbf{P}_k \int dz \frac{\mathbf{n}_i \left(\frac{2k}{(1+z)f}, t(z) \right)}{H(z)(1+z)^6}, \quad (50)$$

where $H(z) \simeq H_0 \sqrt{\Omega_{\text{m}}(1+z)^3 + \Omega_{\text{r}}(1+z)^4}$ for the matter-plus-radiation Universe. Evidently, the amplitude of the SGWB spectrum is strongly determined by the averaged loop power spectrum \mathbf{P}_k emitted in each mode k for a particular loop. We adopt the BOS spectrum [218] with the cusp events dominated on the smooth loops oscillating in the large k mode. For the loop containing cusps, kinks, and kink-kink collisions, \mathbf{P}_k scales as $k^{-4/3}$ [183], $k^{-5/3}$ [219], and k^{-2} [202] respectively. Furthermore, an accurate average power spectrum of loops can be yielded after including the gravitational back reaction. The other key ingredient in Eq. (50) involves the loop number density $\mathbf{n}(\alpha_l, t)$ of the non-self-intersecting, sub-horizon loops of size α_l at the cosmic time $t(z)$. Based on the numerical simulation [220] the

⁴ Infrequent bursts which are negligible for strings satisfying the current pulsar timing limit [216].

TABLE V. The SNRs for the SGWB from cosmic defects, assuming one year operation time.

	string network	cosmic string	
	$N = 3$	$G\mu = 10^{-11}$	$G\mu = 10^{-17}$
TQ (null channel)	5.7×10^{-2}	220	2.5×10^{-1}
TQ I+II (cross-correlation)	1.4×10^{-2}	57	6.4×10^{-2}
TQ+LISA (cross-correlation)	1.9×10^{-2}	45	3.3×10^{-2}

TABLE VI. The order of magnitude range of SNRs for different types of SGWB with TianQin/TianQin+LISA.

Origins	SNR
SBBH+BNS	~ 10
MBHB	$\ll 1$
Phase transition	$< 10^5$
Primordial GW	$\ll 1$
Cosmic defects	$< 10^3$

loop distribution reads [221]

$$\mathbf{n}(\alpha_l, t) = \begin{cases} \frac{0.18}{t^4(\alpha_l + \Gamma G\mu)^{5/2}} \Theta(0.1 - \alpha_l), & (\text{RD}, z \geq z_{\text{eq}}) \\ \frac{0.18(2\sqrt{\Omega_0^0})^{3/2}}{t^{5/2}(\alpha_l + \Gamma G\mu)^{5/2}} (1+z)^3, & z \leq z_{\text{eq}} \\ \frac{0.27 - 0.45\alpha_l^{0.31}}{t^4(\alpha_l + \Gamma G\mu)^2} \Theta(0.18 - \alpha_l), & (\text{MD}, z \leq z_{\text{eq}}), \end{cases} \quad (51)$$

where z_{eq} corresponds to the redshift at matter-radiation equality [222].

As can be seen, the resulting spectrum of the GW emitted by a network of the cosmic strings is sensitive to the various properties of the string network such as (i) the string tension $G\mu$, (ii) the size of cosmic string loops relative to the horizon at birth α_l , and (iii) the cut-off for k_* in the numerical procedure.

In Fig. 10, we show the SGWB from above cosmological sources. We show that TianQin will be sensitive to string tensions with $G\mu \gtrsim 10^{-17}$ for the NG strings, where the upper limit of $G\mu$ is around the value of 10^{-11} [217, 218]. Since the SGWB from cosmic string during RD may presents an oblique rather than flat spectral in the high frequency, it makes cosmic strings an ideal source for probing the expansion history of the Universe [223]. We also show the SNRs for SGWB of the cosmic defects in Tab. V.

V. SUMMARY

In this work, we study the detection prospect of TianQin on various types of SGWB. The SGWB can be roughly divided into two categories: astrophysical-origin and cosmological-origin. We plot the expected signal strength for SGWB of these two categories in Fig. 9 and Fig. 10, respectively,

Due to the huge variance of generation mechanism, the spectra of different sources have distinctive shapes. For example, the SGWB from the cosmic defects appears a nearly scale-invariant spectrum in the TianQin band, the SBBHs and BNSs SGWB spectrum possess a power-law nature, while the SGWB of the PT has a parabolic shape. As a comparison, we also plot the sensitivity curves in the form of PI curves, assuming several configurations, including TianQin, TianQin I+II, and TianQin+LISA.

Most of the astrophysical-origin sources have existing observations to calibrate, therefore, the expected SGWB are accompanied with relatively small uncertainties. On the other hand, the SGWB spectra generated from most cosmological sources have a large theoretical uncertainty in both the amplitude and the peak frequency, even the spectral shape can be quite exotic. This is due to the fact that new physics models beyond the SM that drives the inflation or the PTs typically contain a large amount of the model parameters which have no tight constraints by the current experimental data. Therefore, the preformed analysis at present is qualitatively reliable to estimate the detectability of a GW signal. Notice that in order to probe new physics by means of the GW detection, one has to isolate the SGWB produced from different sources [224, 225].

Among all discussed SGWB, the strongest astrophysical source is expected to be the Galactic DWDs. It can become comparable to the detector noise, thus are sometimes referred to as the foreground. One can suppress the foreground with more observation time and combining more detectors, and for the first time, we discuss a joint foreground with the TianQin-LISA detector network.

In order to detect SGWB, one can use the cross-correlation and null channel methods. The channels within a triangular detector like TianQin and LISA are co-located, and share the same operation time. These factors gains sensitivity to the null channel method. However, the *a priori* knowledge of the noise model needed for the null channel method makes it less appealing than the cross-correlation method. Overall, the cross-correlation method is more robust and reliable, if a simultaneous observation of multiple detectors is possible, like a network of TianQin+LISA or TianQin I+II.

Considering the uncertainties involved in the models, we present a rough range of the expected SNRs for a number of SGWBs in Tab. VI, with an operation time $T_{\text{op}} = 1$ yr assumed. For example, the predicted SGWB from SBBH can differ greatly between the field binary evolution channel [226], the dynamical capture channel [227], and the AGN disk channel [228], since the pre-

dicted eccentricity distribution can be wildly different. Therefore, the observation of astronomical sources will help us greatly advance in our understanding of the compact binary population properties. While for the much less certain cosmological sources, their observations will obviously celebrate the long waited breakthrough of the new physics beyond standard model. However, even a null observation can still help to place important upper limit on corresponding models and better guide the theoretical development.

Recently, the NANOGrav team reported an interesting observation from their 12.5 year data, where strong evidence points to the existence of a stochastic process that can not be explained by noise. However, the lack of the quadrupolar spatial correlation made the team restrained to directly claim the detection of a SGWB [152]. This discovery added credibility to the study of SGWB, and we believe that the opening up of the mHz GW window would certainly trigger a huge spike in the understanding of underling physics behind the future SGWB detec-

tions. Furthormore, with the increasing of sensitivity in the nano-Hertz frequency band, as well as the opening of high frequency band of the GW window, we can expect to use multi-band GW observation to better constrain our understanding of SGWBs [229].

ACKNOWLEDGMENTS

This work has been supported by the National Key Research and Development Program of China (No. 2020YFC2201400), and the Natural Science Foundation of China (Grants No. 11805286, 11690022). Y. J. is supported by the GuangDong Basic and Applied Basic Research Foundation (No. 2020A1515110150). We would like to thank Valeriya Korol for providing the sample of Galaxy DWD. We also thank Neil Cornish, Yi-Fan Wang, Shun-Jia Huang, Hai-Tian Wang, Xiang-Yu Lyu, Bo-Bing Ye, En-Kun Li and Fa-Peng Huang for helpful discussions.

Appendix A: Coordinates for TianQin and LISA

When calculating ORF of TianQin + LISA, it need to construct the uniform coordinate system for TianQin and LISA. In the coordinate system where the x axis points in the direction of the vernal equinox,

The ecliptic coordinate for TianQin is given by two parts, the ecliptic coordinate for the center of the Earth is given by:

$$\begin{aligned} X(t) &= R \cos(\alpha_{\text{TQ}}(t)) + \frac{1}{2}eR(\cos(2\alpha_{\text{TQ}}(t)) - 3) + O(e^2) \\ Y(t) &= R \sin(\alpha_{\text{TQ}}(t)) + \frac{1}{2}eR \sin(2\alpha_{\text{TQ}}(t)) + O(e^2) \\ Z(t) &= 0, \end{aligned} \tag{A1}$$

where $e = 0.0167$, $R = 1 \text{ AU}$, $\alpha_{\text{TQ}}(t) = 2\pi f_{\text{m}}t - \beta$, $f_{\text{m}} = 1/\text{yr}$, the longitude of the perihelion $\beta = 102.9^\circ$. And the geocentric-ecliptic coordinate for TianQin is given by:

$$\begin{aligned} \tilde{x}_n(t) &= R_1(\cos \phi_s \sin \theta_s \sin \alpha_n + \cos \alpha_n \sin \phi_s) \\ \tilde{y}_n(t) &= R_1(\sin \phi_s \sin \theta_s \sin \alpha_n - \cos \alpha_n \cos \phi_s) \\ \tilde{z}_n(t) &= -R_1 \sin \alpha_n \cos \theta_s, \end{aligned} \tag{A2}$$

where $\alpha_n = 2\pi f_{\text{sc}}t + \kappa_n$ with $\kappa_n = \frac{2}{3}(n-1)\pi$, $R_1 = 1 \times 10^5 \text{ km}$, $\theta_s = -4.7^\circ$, $\phi_s = 120.5^\circ$, $f_{\text{sc}} = 1/(3.64 \text{ days})$, $n = 1, 2, 3$, which denotes the three satellites of TianQin.

By adding Eq. (A1) and Eq. (A2), the ecliptic coordinate for the three satellites are attained.

One the other hand, the ecliptic coordinate for LISA are written as:

$$\begin{aligned} x'_n(t) &= R \cos(\alpha_{\text{LISA}}(t)) + \frac{1}{2}eR(\cos(2\alpha_{\text{LISA}}(t) - \kappa_n) \\ &\quad - 3 \cos \kappa_n) \\ y'_n(t) &= R \sin(\alpha_{\text{LISA}}(t)) + \frac{1}{2}eR(\sin(2\alpha_{\text{LISA}}(t) - \kappa_n) \\ &\quad - 3 \sin \kappa_n) \\ z'_n(t) &= -\sqrt{3}eR \cos(\alpha'_n(t) - \kappa_n), \end{aligned} \tag{A3}$$

where $\alpha_{\text{LISA}}(t) = 2\pi f_{\text{m}}t - \beta + \Delta\alpha$ with $\kappa_n = \frac{2}{3}(n-1)\pi$ with the relative phase $\Delta\alpha \simeq 20^\circ$, $e = 0.0048$, $R = 1 \text{ AU}$.

Appendix B: Some derivations for null channel

When adopting the null channel, the estimator is constructed by:

$$K = \sum_{I=A,E} \int_{-T/2}^{T/2} dt \int_{-\infty}^{\infty} dt' \int_{-\infty}^{\infty} df \int_{-\infty}^{\infty} df' \tilde{h}_I(f) \tilde{h}_I^*(f') Q(t' - t) e^{-i2\pi f'(t'-t)} e^{-i2\pi(f'-f)t}$$

Then the estimator for the SGWB signal is:

$$\begin{aligned} \mu &:= \langle K \rangle \\ &= \sum_{I=A,E} \int_{-T/2}^{T/2} dt \int_{-\infty}^{\infty} dt' \int_{-\infty}^{\infty} df \int_{-\infty}^{\infty} df' \langle \tilde{h}_I(f) \tilde{h}_I^*(f') \rangle Q(t' - t) e^{-i2\pi f'(t'-t)} e^{-i2\pi(f'-f)t} \\ &= \sum_{I=A,E} \int_{-T/2}^{T/2} dt \int_{-\infty}^{\infty} df \int_{-\infty}^{\infty} df' \langle \tilde{h}_I(f) \tilde{h}_I^*(f') \rangle \tilde{Q}(f) e^{-i2\pi(f'-f)t} \\ &= 2T \int_0^{\infty} df \Gamma_{II}(f) S_h(f) \tilde{Q}(f), \end{aligned} \tag{B1}$$

as for the noise contribution:

$$\begin{aligned} \sigma^2 &\approx \langle K(t, t')^2 \rangle \\ &= \sum_{I=A,E} \sum_{J=A,E} \int_{-T/2}^{T/2} dt \int_{-\infty}^{\infty} dt' \int_{-T/2}^{T/2} d\eta \int_{-\infty}^{\infty} d\eta' \int_{-\infty}^{\infty} df \int_{-\infty}^{\infty} df' \int_{-\infty}^{\infty} dk \int_{-\infty}^{\infty} dk' \\ &\times \left[\left\langle \left(\tilde{n}_I(f) \tilde{n}_I^*(f') - z_I(f) \tilde{n}_T(f) \tilde{n}_T^*(f') \right) \left(\tilde{n}_J(k) \tilde{n}_J^*(k') - z_J(k) \tilde{n}_T(k) \tilde{n}_T^*(k') \right) \right\rangle \right] \\ &\times Q(t' - t) e^{-i2\pi f'(t'-t)} Q(\eta' - \eta) e^{-i2\pi k'(\eta' - \eta)} e^{i2\pi f'(t'-t)} e^{i2\pi k(\eta' - \eta)} e^{i2\pi f t} e^{-i2\pi f' t'} e^{i2\pi k \eta} e^{-i2\pi k' \eta'} \\ &= \sum_{I=A,E} \sum_{J=A,E} \int_{-T/2}^{T/2} dt \int_{-T/2}^{T/2} d\eta \int_{-\infty}^{\infty} df \int_{-\infty}^{\infty} df' \int_{-\infty}^{\infty} dk \int_{-\infty}^{\infty} dk' \left[\langle \tilde{n}_I(f) \tilde{n}_J(k) \rangle \langle \tilde{n}_I^*(f') \tilde{n}_J^*(k') \rangle \right. \\ &\left. + \langle \tilde{n}_I(f) \tilde{n}_J^*(k') \rangle \langle \tilde{n}_J(k) \tilde{n}_I^*(f') \rangle \right] \tilde{Q}(f') \tilde{Q}(k') e^{-i2\pi(f'-f)t} e^{-i2\pi(k'-k)\eta} \\ &= \int_{-T/2}^{T/2} dt \int_{-\infty}^{\infty} df \int_{-\infty}^{\infty} df' \frac{1}{2} \delta(f - f') P_{n_I}(|f|) P_{n_I}(|f'|) \tilde{Q}(f) \tilde{Q}(-f') e^{-i2\pi(f'-f)t} \\ &= 2T \int_0^{\infty} df P_{n_I}^2(f) |\tilde{Q}(f)|^2, \end{aligned} \tag{B2}$$

when the filter function is written as

$$\tilde{Q}(f) = \frac{\Gamma_{II}^{\text{TQ}}(|f|) S_h(|f|)}{P_{n_I}^2(|f|)}, \tag{B3}$$

the SNR for the null channel obtain the optimal value.

-
- [1] M. Maggiore, *Phys. Rept.* **331**, 283 (2000), [arXiv:gr-qc/9909001 \[gr-qc\]](#).
[2] N. Christensen, *Rept. Prog. Phys.* **82**, 016903 (2019), [arXiv:1811.08797 \[gr-qc\]](#).
[3] J. D. Romano (2019) [arXiv:1909.00269 \[gr-qc\]](#).
[4] J. C. N. de Araujo, O. D. Miranda, and O. D. Aguiar, *Phys. Rev. D* **61**, 124015 (2000), [arXiv:astro-ph/0004395](#).
[5] K. Martinovic, P. M. Meyers, M. Sakellariadou, and N. Christensen, *Phys. Rev. D* **103**, 043023 (2021), [arXiv:2011.05697 \[gr-qc\]](#).
[6] P. Amaro-Seoane *et al.* (LISA), (2017), [arXiv:1702.00786 \[astro-ph.IM\]](#).
[7] V. Korol, E. M. Rossi, P. J. Groot, G. Nelemans, S. Toonen, and A. G. A. Brown, *Mon. Not. Roy. Astron. Soc.* **470**, 1894 (2017), [arXiv:1703.02555 \[astro-ph.HE\]](#).

- [8] S.-J. Huang, Y.-M. Hu, V. Korol, P.-C. Li, Z.-C. Liang, Y. Lu, H.-T. Wang, S. Yu, and J. Mei, *Phys. Rev. D* **102**, 063021 (2020), arXiv:2005.07889 [astro-ph.HE].
- [9] H.-T. Wang, Z. Jiang, A. Sesana, E. Barausse, S.-J. Huang, Y.-F. Wang, W.-F. Feng, Y. Wang, Y.-M. Hu, J. Mei, and J. Luo, *Phys. Rev. D* **100**, 043003 (2019), arXiv:1902.04423 [astro-ph.HE].
- [10] S. Liu, Y.-M. Hu, J.-d. Zhang, and J. Mei, *Phys. Rev. D* **101**, 103027 (2020), arXiv:2004.14242 [astro-ph.HE].
- [11] H.-M. Fan, Y.-M. Hu, E. Barausse, A. Sesana, J.-d. Zhang, X. Zhang, T.-G. Zi, and J. Mei, *Phys. Rev. D* **102**, 063016 (2020), arXiv:2005.08212 [astro-ph.HE].
- [12] T.-G. Zi, J.-D. Zhang, H.-M. Fan, X.-T. Zhang, Y.-M. Hu, C. Shi, and J. Mei, (2021), arXiv:2104.06047 [gr-qc].
- [13] A. H. Guth and S. Y. Pi, *Phys. Rev. Lett.* **49**, 1110 (1982).
- [14] C. J. Hogan, *Phys. Lett. B* **133**, 172 (1983).
- [15] T. W. B. Kibble, *J. Phys. A* **9**, 1387 (1976).
- [16] N. Mazumder, S. Mitra, and S. Dhurandhar, *Phys. Rev. D* **89**, 084076 (2014), arXiv:1401.5898 [gr-qc].
- [17] T. Callister, L. Sammut, S. Qiu, I. Mandel, and E. Thrane, *Phys. Rev. X* **6**, 031018 (2016), arXiv:1604.02513 [gr-qc].
- [18] A. Maselli, S. Marassi, V. Ferrari, K. Kokkotas, and R. Schneider, *Phys. Rev. Lett.* **117**, 091102 (2016), arXiv:1606.04996 [gr-qc].
- [19] K. Breivik, C. M. F. Mingarelli, and S. L. Larson, *Astrophys. J.* **901**, 4 (2020), arXiv:1912.02200 [astro-ph.GA].
- [20] M. Maggiore, ICTP Lect. Notes Ser. **3**, 397 (2001), arXiv:gr-qc/0008027.
- [21] C. Ungarelli and A. Vecchio, *Phys. Rev. D* **63**, 064030 (2001), arXiv:gr-qc/0003021.
- [22] P. Amaro-Seoane *et al.*, *GW Notes* **6**, 4 (2013), arXiv:1201.3621 [astro-ph.CO].
- [23] D. Hils, P. L. Bender, and R. F. Webbink, *Astrophys. J.* **360**, 75 (1990).
- [24] P. Amaro-Seoane *et al.*, *Class. Quant. Grav.* **29**, 124016 (2012), arXiv:1202.0839 [gr-qc].
- [25] S. Nissanke, M. Vallisneri, G. Nelemans, and T. A. Prince, *Astrophys. J.* **758**, 131 (2012), arXiv:1201.4613 [astro-ph.GA].
- [26] G. Nelemans, ASP Conf. Ser. **467**, 27 (2013), arXiv:1302.0138 [astro-ph.HE].
- [27] M. Benacquista, *Proceedings, IAU Symposium 312: Star Clusters and Black Holes in Galaxies across Cosmic Time: Beijing, China, August 25-29, 2014, IAU Symp.* **312**, 289 (2016).
- [28] M. R. Adams and N. J. Cornish, *Phys. Rev. D* **89**, 022001 (2014), arXiv:1307.4116 [gr-qc].
- [29] P. L. Bender and D. Hils, *Class. Quant. Grav.* **14**, 1439 (1997).
- [30] G. Nelemans, L. R. Yungelson, and S. F. Portegies Zwart, *Astron. Astrophys.* **375**, 890 (2001), arXiv:astro-ph/0105221.
- [31] L. Barack and C. Cutler, *Phys. Rev. D* **70**, 122002 (2004), arXiv:gr-qc/0409010.
- [32] J. A. Edlund, M. Tinto, A. Krolak, and G. Nelemans, *Phys. Rev. D* **71**, 122003 (2005), arXiv:gr-qc/0504112.
- [33] A. J. Ruiter, K. Belczynski, M. Benacquista, S. L. Larson, and G. Williams, *Astrophys. J.* **717**, 1006 (2010), arXiv:0705.3272 [astro-ph].
- [34] G. Nelemans, *Class. Quant. Grav.* **26**, 094030 (2009), arXiv:0901.1778 [astro-ph.SR].
- [35] J. Luo *et al.* (TianQin), *Class. Quant. Grav.* **33**, 035010 (2016), arXiv:1512.02076 [astro-ph.IM].
- [36] S. Kawamura *et al.*, *Class. Quant. Grav.* **28**, 094011 (2011).
- [37] J. Crowder and N. J. Cornish, *Phys. Rev. D* **72**, 083005 (2005), arXiv:gr-qc/0506015.
- [38] W.-R. Hu and Y.-L. Wu, *Natl. Sci. Rev.* **4**, 685 (2017).
- [39] Z. Tan, B. Ye, and X. Zhang, *Int. J. Mod. Phys. D* **29**, 08 (2020), arXiv:2012.03261 [gr-qc].
- [40] J. Mei *et al.* (TianQin), (2020), 10.1093/ptep/ptaa114, arXiv:2008.10332 [gr-qc].
- [41] C. Shi, J. Bao, H.-T. Wang, J.-d. Zhang, Y.-M. Hu, A. Sesana, E. Barausse, J. Mei, and J. Luo, *Phys. Rev. D* **100**, 044036 (2019), arXiv:1902.08922 [gr-qc].
- [42] J. Bao, C. Shi, H. Wang, J.-d. Zhang, Y. Hu, J. Mei, and J. Luo, *Phys. Rev. D* **100**, 084024 (2019), arXiv:1905.11674 [gr-qc].
- [43] N. Wiener, *Extrapolation, Interpolation, and Smoothing of Stationary Time Series* (The MIT Press, 1964).
- [44] B. J. Owen and B. S. Sathyaprakash, *Phys. Rev. D* **60**, 022002 (1999), arXiv:gr-qc/9808076.
- [45] B. Allen and J. D. Romano, *Phys. Rev. D* **59**, 102001 (1999), arXiv:gr-qc/9710117 [gr-qc].
- [46] M. Tinto, J. W. Armstrong, and F. B. Estabrook, *Phys. Rev. D* **63**, 021101 (2001).
- [47] M. Tinto, F. B. Estabrook, and J. W. Armstrong, *Phys. Rev. D* **65**, 082003 (2002).
- [48] C. J. Hogan and P. L. Bender, *Phys. Rev. D* **64**, 062002 (2001), arXiv:astro-ph/0104266.
- [49] T. A. Prince, M. Tinto, S. L. Larson, and J. W. Armstrong, *Phys. Rev. D* **66**, 122002 (2002), arXiv:gr-qc/0209039.
- [50] M. Tinto and S. V. Dhurandhar, *Living Rev. Rel.* **8**, 4 (2005), arXiv:gr-qc/0409034.
- [51] R. Hellings and G. Downs, *Astrophys. J. Lett.* **265**, L39 (1983).
- [52] N. Christensen, *Phys. Rev. D* **46**, 5250 (1992).
- [53] E. E. Flanagan, *Phys. Rev. D* **48**, 2389 (1993), arXiv:astro-ph/9305029 [astro-ph].
- [54] M. R. Adams and N. J. Cornish, *Phys. Rev. D* **82**, 022002 (2010), arXiv:1002.1291 [gr-qc].
- [55] E. L. Robinson, J. D. Romano, and A. Vecchio, *Proceedings, 12th Workshop on Gravitational wave data analysis (GWDAA-12): Cambridge, USA, December 13-16, 2007, Class. Quant. Grav.* **25**, 184019 (2008), arXiv:0804.4144 [gr-qc].
- [56] J. D. Romano and N. J. Cornish, *Living Rev. Rel.* **20**, 2 (2017), arXiv:1608.06889 [gr-qc].
- [57] B. F. Schutz, *Class. Quant. Grav.* **16**, A131 (1999), arXiv:gr-qc/9911034.
- [58] B. Allen and A. C. Ottewill, *Phys. Rev. D* **56**, 545 (1997), arXiv:gr-qc/9607068.
- [59] N. Aghanim *et al.* (Planck), *Astron. Astrophys.* **641**, A6 (2020), arXiv:1807.06209 [astro-ph.CO].
- [60] B. Allen, in *Relativistic gravitation and gravitational radiation. Proceedings, School of Physics, Les Houches, France, September 26-October 6, 1995* (1996) pp. 373–417, arXiv:gr-qc/9604033 [gr-qc].
- [61] C. Cutler and E. E. Flanagan, *Phys. Rev. D* **49**, 2658 (1994), arXiv:gr-qc/9402014.
- [62] N. J. Cornish and S. L. Larson, *Class. Quant. Grav.* **18**, 3473 (2001), arXiv:gr-qc/0103075.
- [63] B. P. Abbott, R. Abbott, T. D. Abbott, M. R. Aber-

- nathy, F. Acernese, K. Ackley, C. Adams, T. Adams, P. Addresso, R. X. Adhikari, and et al., *Phys. Rev. Lett.* **116**, 241103 (2016), arXiv:1606.04855 [gr-qc].
- [64] J. D. E. Creighton and W. G. Anderson, *Gravitational-wave physics and astronomy: An introduction to theory, experiment and data analysis* (2011).
- [65] C. W. Misner, K. S. Thorne, and J. A. Wheeler, *Gravitation* (W. H. Freeman, San Francisco, 1973).
- [66] J. D. Romano and N. J. Cornish, *Living Reviews in Relativity* **20**, 2 (2017), arXiv:1608.06889 [gr-qc].
- [67] N. J. Cornish, *Phys. Rev.* **D65**, 022004 (2002), arXiv:gr-qc/0106058 [gr-qc].
- [68] N. J. Cornish and L. J. Rubbo, *Phys. Rev. D* **67**, 029905 (2003), arXiv:gr-qc/0209011 [gr-qc].
- [69] B. Abbott *et al.* (ALLEGRO, LIGO Scientific), *Phys. Rev. D* **76**, 022001 (2007), arXiv:gr-qc/0703068.
- [70] L. S. Finn, S. L. Larson, and J. D. Romano, *Phys. Rev. D* **79**, 062003 (2009), arXiv:0811.3582 [gr-qc].
- [71] A. Nishizawa and K. Hayama, *Phys. Rev. D* **88**, 064005 (2013), arXiv:1307.1281 [gr-qc].
- [72] B. Ye, X. Zhang, Y. Ding, and Y. Meng, *Phys. Rev. D* **103**, 042007 (2021), arXiv:2012.03269 [gr-qc].
- [73] P. Ajith, M. Hewitson, and I. S. Heng, *Class. Quant. Grav.* **23**, S741 (2006), arXiv:gr-qc/0604004.
- [74] T. Robson, N. J. Cornish, and C. Liu, *Classical and Quantum Gravity* **36**, 105011 (2019), arXiv:1803.01944 [astro-ph.HE].
- [75] L. S. Finn, *Phys. Rev. D* **46**, 5236 (1992), arXiv:gr-qc/9209010.
- [76] A. A. Penzias and R. W. Wilson, *Astrophys. J.* **142**, 419 (1965).
- [77] J. T. Whelan, *Class. Quant. Grav.* **23**, 1181 (2006), arXiv:gr-qc/0509109.
- [78] S. Bose, *Phys. Rev. D* **71**, 082001 (2005), arXiv:astro-ph/0504048.
- [79] B. P. Abbott *et al.* (LIGO Scientific, VIRGO), *Nature* **460**, 990 (2009), arXiv:0910.5772 [astro-ph.CO].
- [80] T. Regimbau, D. Meacher, and M. Coughlin, *Phys. Rev. D* **89**, 084046 (2014), arXiv:1404.1134 [astro-ph.CO].
- [81] J. Aasi *et al.* (LIGO Scientific, VIRGO), *Phys. Rev. Lett.* **113**, 231101 (2014), arXiv:1406.4556 [gr-qc].
- [82] J. Aasi *et al.* (LIGO Scientific, VIRGO), *Phys. Rev. D* **91**, 022003 (2015), arXiv:1410.6211 [gr-qc].
- [83] D. Meacher, M. Coughlin, S. Morris, T. Regimbau, N. Christensen, S. Kandhasamy, V. Mandic, J. D. Romano, and E. Thrane, *Phys. Rev. D* **92**, 063002 (2015), arXiv:1506.06744 [astro-ph.HE].
- [84] A. Nishizawa and N. Seto, *J. Phys. Conf. Ser.* **716**, 012013 (2016).
- [85] B. P. Abbott *et al.* (LIGO Scientific, Virgo), *Phys. Rev. Lett.* **118**, 121101 (2017), [Erratum: *Phys.Rev.Lett.* **119**, 029901 (2017)], arXiv:1612.02029 [gr-qc].
- [86] B. P. Abbott *et al.* (LIGO Scientific, Virgo), *Phys. Rev. D* **100**, 061101 (2019), arXiv:1903.02886 [gr-qc].
- [87] N. Seto, *Phys. Rev. D* **102**, 123547 (2020), arXiv:2010.06877 [gr-qc].
- [88] R. Abbott *et al.* (LIGO Scientific, Virgo, KAGRA), (2021), arXiv:2101.12130 [gr-qc].
- [89] P. F. Michelson, *Monthly Notices of the Royal Astronomical Society* **227**, 933 (1987), <https://academic.oup.com/mnras/article-pdf/227/4/933/3926536/mnras227-0933.pdf>.
- [90] S. Vitale, M. Cerdonio, E. Coccia, and A. Ortolan, *Phys. Rev. D* **55**, 1741 (1997), arXiv:astro-ph/9611088.
- [91] B. Allen and R. Brustein, *Phys. Rev. D* **55**, 3260 (1997), arXiv:gr-qc/9609013.
- [92] M. Rakhmanov, J. D. Romano, and J. T. Whelan, *Class. Quant. Grav.* **25**, 184017 (2008), arXiv:0808.3805 [gr-qc].
- [93] S. V. Dhurandhar, K. Rajesh Nayak, and J. Y. Vinet, *Phys. Rev. D* **65**, 102002 (2002), arXiv:gr-qc/0112059.
- [94] C. Cutler, *Phys. Rev. D* **57**, 7089 (1998), arXiv:gr-qc/9703068.
- [95] D. Meacher, E. Thrane, and T. Regimbau, *Phys. Rev. D* **89**, 084063 (2014), arXiv:1402.6231 [astro-ph.CO].
- [96] B. S. Sathyaprakash and S. V. Dhurandhar, *Phys. Rev. D* **44**, 3819 (1991).
- [97] A. Sharma and J. Harms, *Phys. Rev. D* **102**, 063009 (2020), arXiv:2006.16116 [gr-qc].
- [98] X.-C. Hu, X.-H. Li, Y. Wang, W.-F. Feng, M.-Y. Zhou, Y.-M. Hu, S.-C. Hu, J.-W. Mei, and C.-G. Shao, *Classical and Quantum Gravity* **35**, 095008 (2018), arXiv:1803.03368 [gr-qc].
- [99] N. J. Cornish and L. J. Rubbo, *Phys. Rev. D* **67**, 022001 (2003), [Erratum: *Phys.Rev.D* **67**, 029905 (2003)], arXiv:gr-qc/0209011.
- [100] M. Tinto, D. A. Shaddock, J. Sylvestre, and J. W. Armstrong, *Phys. Rev.* **D67**, 122003 (2003), arXiv:gr-qc/0303013 [gr-qc].
- [101] M. Tinto, F. B. Estabrook, and J. W. Armstrong, *Phys. Rev.* **D69**, 082001 (2004), arXiv:gr-qc/0310017 [gr-qc].
- [102] M. Vallisneri, *Phys. Rev.* **D71**, 022001 (2005), arXiv:gr-qc/0407102 [gr-qc].
- [103] M. Tinto, M. Vallisneri, and J. W. Armstrong, *Phys. Rev.* **D71**, 041101 (2005), arXiv:gr-qc/0410122 [gr-qc].
- [104] T. L. Smith and R. Caldwell, *Phys. Rev.* **D100**, 104055 (2019), arXiv:1908.00546 [astro-ph.CO].
- [105] X.-Y. Lu, Y.-J. Tan, and C.-G. Shao, *Phys. Rev. D* **100**, 044042 (2019).
- [106] A. Krolak, M. Tinto, and M. Vallisneri, *Phys. Rev. D* **70**, 022003 (2004), [Erratum: *Phys.Rev.D* **76**, 069901 (2007)], arXiv:gr-qc/0401108.
- [107] H. Kudoh, A. Taruya, T. Hiramatsu, and Y. Himemoto, *Phys. Rev. D* **73**, 064006 (2006), arXiv:gr-qc/0511145.
- [108] E. Thrane, N. Christensen, R. M. S. Schofield, and A. Effler, *Phys. Rev. D* **90**, 023013 (2014), arXiv:1406.2367 [astro-ph.IM].
- [109] E. Thrane and J. D. Romano, *Phys. Rev.* **D88**, 124032 (2013), arXiv:1310.5300 [astro-ph.IM].
- [110] K. Schmitz, *JHEP* **01**, 097 (2021), arXiv:2002.04615 [hep-ph].
- [111] A. Buonanno, Y.-b. Chen, and M. Vallisneri, *Phys. Rev. D* **67**, 024016 (2003), [Erratum: *Phys.Rev.D* **74**, 029903 (2006)], arXiv:gr-qc/0205122.
- [112] C. J. Moore, D. Gerosa, and A. Klein, *Mon. Not. Roy. Astron. Soc.* **488**, L94 (2019), arXiv:1905.11998 [astro-ph.HE].
- [113] C. Caprini *et al.*, *JCAP* **03**, 024 (2020), arXiv:1910.13125 [astro-ph.CO].
- [114] M. Giovannini, *Prog. Part. Nucl. Phys.* **112**, 103774 (2020), arXiv:1912.07065 [astro-ph.CO].
- [115] D. Poletti, *JCAP* **05**, 052 (2021), arXiv:2101.02713 [gr-qc].
- [116] K. A. Postnov and M. E. Prokhorov, *Astrophys. J.* **494**, 674 (1998), arXiv:astro-ph/9801034.
- [117] T. Regimbau and J. A. de Freitas Pacheco, *Astrophys. J.* **642**, 455 (2006), arXiv:gr-qc/0512008.

- [118] C. Wu, V. Mandic, and T. Regimbau, *Phys. Rev.* **D85**, 104024 (2012), arXiv:1112.1898 [gr-qc].
- [119] X.-J. Zhu, E. Howell, T. Regimbau, D. Blair, and Z.-H. Zhu, *Astrophys. J.* **739**, 86 (2011), arXiv:1104.3565 [gr-qc].
- [120] I. Cholis, *JCAP* **06**, 037 (2017), arXiv:1609.03565 [astro-ph.HE].
- [121] Z.-C. Chen, F. Huang, and Q.-G. Huang, *Astrophys. J.* **871**, 97 (2019), arXiv:1809.10360 [gr-qc].
- [122] D. S. Salopek and J. R. Bond, *Phys. Rev. D* **43**, 1005 (1991).
- [123] S. R. Coleman, *Phys. Rev. D* **15**, 2929 (1977), [Erratum: *Phys.Rev.D* 16, 1248 (1977)].
- [124] A. Albrecht and N. Turok, *Phys. Rev. Lett.* **54**, 1868 (1985).
- [125] D. Hils, P. L. Bender, and R. F. Webbink, *Astrophys. J.* **360**, 75 (1990).
- [126] G. Nelemans and C. A. Tout, *Mon. Not. Roy. Astron. Soc.* **356**, 753 (2005), arXiv:astro-ph/0410301 [astro-ph].
- [127] N. Cornish and T. Robson, *Proceedings, 11th International LISA Symposium: Zurich, Switzerland, September 5-9, 2016*, *J. Phys. Conf. Ser.* **840**, 012024 (2017), arXiv:1703.09858 [astro-ph.IM].
- [128] N. J. Cornish and T. B. Littenberg, *Phys. Rev. D* **76**, 083006 (2007), arXiv:0704.1808 [gr-qc].
- [129] T. Robson and N. Cornish, *Class. Quant. Grav.* **34**, 244002 (2017), arXiv:1705.09421 [gr-qc].
- [130] J. Harms, C. Mahrtdt, M. Otto, and M. Priess, *Phys. Rev. D* **77**, 123010 (2008), arXiv:0803.0226 [gr-qc].
- [131] S. Ma, Z. Cao, C.-Y. Lin, H.-P. Pan, and H.-J. Yo, *Phys. Rev. D* **96**, 084046 (2017), arXiv:1710.02965 [gr-qc].
- [132] G. Wang and W.-B. Han, *Phys. Rev. D* **103**, 064021 (2021), arXiv:2101.01991 [gr-qc].
- [133] B. Abbott *et al.* (LIGO Scientific, Virgo), *Phys. Rev. X* **9**, 031040 (2019), arXiv:1811.12907 [astro-ph.HE].
- [134] B. Abbott *et al.* (LIGO Scientific, Virgo), *Astrophys. J. Lett.* **892**, L3 (2020), arXiv:2001.01761 [astro-ph.HE].
- [135] R. Abbott *et al.* (LIGO Scientific, Virgo), *Phys. Rev. D* **102**, 043015 (2020), arXiv:2004.08342 [astro-ph.HE].
- [136] R. Abbott *et al.* (LIGO Scientific, Virgo), *Astrophys. J. Lett.* **896**, L44 (2020), arXiv:2006.12611 [astro-ph.HE].
- [137] R. Abbott *et al.* (LIGO Scientific, Virgo), *Phys. Rev. Lett.* **125**, 101102 (2020), arXiv:2009.01075 [gr-qc].
- [138] A. Sesana, *Phys. Rev. Lett.* **116**, 231102 (2016), arXiv:1602.06951 [gr-qc].
- [139] Y. M. Hu, J. Mei, and J. Luo, *National Science Review* **4**, 683 (2017).
- [140] B. Abbott *et al.* (LIGO Scientific, Virgo), *Phys. Rev. Lett.* **116**, 131102 (2016), arXiv:1602.03847 [gr-qc].
- [141] B. P. Abbott *et al.* (LIGO Scientific, Virgo), *Phys. Rev. Lett.* **120**, 091101 (2018), arXiv:1710.05837 [gr-qc].
- [142] I. Dvorkin, E. Vangioni, J. Silk, J.-P. Uzan, and K. A. Olive, *Mon. Not. Roy. Astron. Soc.* **461**, 3877 (2016), arXiv:1604.04288 [astro-ph.HE].
- [143] K. Nakazato, Y. Niino, and N. Sago, *Astrophys. J.* **832**, 146 (2016), arXiv:1605.02146 [astro-ph.HE].
- [144] K. Inayoshi, K. Kashiyama, E. Visbal, and Z. Haiman, *Mon. Not. Roy. Astron. Soc.* **461**, 2722 (2016), arXiv:1603.06921 [astro-ph.GA].
- [145] R. Abbott *et al.* (LIGO Scientific, Virgo), (2020), arXiv:2010.14533 [astro-ph.HE].
- [146] B. P. Abbott *et al.* (LIGO Scientific, Virgo), *Astrophys. J.* **882**, L24 (2019), arXiv:1811.12940 [astro-ph.HE].
- [147] B. Abbott *et al.* (LIGO Scientific, Virgo), *Phys. Rev. X* **6**, 041015 (2016), [Erratum: *Phys.Rev.X* 8, 039903 (2018)], arXiv:1606.04856 [gr-qc].
- [148] C. P erigois, C. Belczynski, T. Bulik, and T. Regimbau, (2020), arXiv:2008.04890 [astro-ph.CO].
- [149] P. Ajith *et al.*, *Phys. Rev. Lett.* **106**, 241101 (2011), arXiv:0909.2867 [gr-qc].
- [150] L. Z. Kelley, L. Blecha, L. Hernquist, A. Sesana, and S. R. Taylor, *Mon. Not. Roy. Astron. Soc.* **471**, 4508 (2017), arXiv:1702.02180 [astro-ph.HE].
- [151] I. Dvorkin and E. Barausse, *Mon. Not. Roy. Astron. Soc.* **470**, 4547 (2017), arXiv:1702.06964 [astro-ph.GA].
- [152] Z. Arzoumanian *et al.* (NANOGrav), (2020), arXiv:2009.04496 [astro-ph.HE].
- [153] W.-F. Feng, H.-T. Wang, X.-C. Hu, Y.-M. Hu, and Y. Wang, *Phys. Rev. D* **99**, 123002 (2019), arXiv:1901.02159 [astro-ph.IM].
- [154] A. Sesana, F. Haardt, P. Madau, and M. Volonteri, *Astrophys. J.* **623**, 23 (2005), arXiv:astro-ph/0409255 [astro-ph].
- [155] A. Sesana, M. Volonteri, and F. Haardt, *Mon. Not. Roy. Astron. Soc.* **377**, 1711 (2007), arXiv:astro-ph/0701556.
- [156] A. Sesana, A. Vecchio, and C. N. Colacino, *Mon. Not. Roy. Astron. Soc.* **390**, 192 (2008), arXiv:0804.4476 [astro-ph].
- [157] V. Ferrari, S. Matarrese, and R. Schneider, *Mon. Not. Roy. Astron. Soc.* **303**, 247 (1999), arXiv:astro-ph/9804259.
- [158] K. Crocker, T. Prestegard, V. Mandic, T. Regimbau, K. Olive, and E. Vangioni, *Phys. Rev. D* **95**, 063015 (2017), arXiv:1701.02638 [astro-ph.CO].
- [159] B. J. Owen, L. Lindblom, C. Cutler, B. F. Schutz, A. Vecchio, and N. Andersson, *Phys. Rev. D* **58**, 084020 (1998), arXiv:gr-qc/9804044.
- [160] P. A. Rosado, *Phys. Rev. D* **86**, 104007 (2012), arXiv:1206.1330 [gr-qc].
- [161] S. Marassi, R. Ciolfi, R. Schneider, L. Stella, and V. Ferrari, *Mon. Not. Roy. Astron. Soc.* **411**, 2549 (2011), arXiv:1009.1240 [astro-ph.CO].
- [162] Q. Cheng, S.-N. Zhang, and X.-P. Zheng, *Phys. Rev. D* **95**, 083003 (2017), arXiv:1704.02013 [astro-ph.HE].
- [163] L. P. Grishchuk, *Soviet Journal of Experimental and Theoretical Physics Letters* **23**, 293 (1976).
- [164] A. A. Starobinsky, *JETP Lett.* **30**, 682 (1979).
- [165] D. Polarski and A. A. Starobinsky, *Class. Quant. Grav.* **13**, 377 (1996), arXiv:gr-qc/9504030.
- [166] M. C. Guzzetti, N. Bartolo, M. Liguori, and S. Matarrese, *Riv. Nuovo Cim.* **39**, 399 (2016), arXiv:1605.01615 [astro-ph.CO].
- [167] R. H. Brandenberger, in *IPM School on Cosmology 1999: Large Scale Structure Formation* (1999) arXiv:hep-ph/9910410.
- [168] M. Maggiore, *Gravitational Waves. Vol. 2: Astrophysics and Cosmology* (Oxford University Press, 2018).
- [169] W. Hu and S. Dodelson, *Ann. Rev. Astron. Astrophys.* **40**, 171 (2002), arXiv:astro-ph/0110414.
- [170] Y. Akrami *et al.* (Planck), (2018), arXiv:1807.06211 [astro-ph.CO].
- [171] C. Caprini and D. G. Figueroa, *Class. Quant. Grav.* **35**, 163001 (2018), arXiv:1801.04268 [astro-ph.CO].
- [172] J. Ellis, M. Lewicki, J. M. No, and V. Vaskonen, *JCAP* **06**, 024 (2019), arXiv:1903.09642 [hep-ph].
- [173] D. Baumann, P. J. Steinhardt, K. Takahashi, and

- K. Ichiki, *Phys. Rev. D* **76**, 084019 (2007), arXiv:hep-th/0703290.
- [174] C. Cheung, P. Creminelli, A. L. Fitzpatrick, J. Kaplan, and L. Senatore, *JHEP* **03**, 014 (2008), arXiv:0709.0293 [hep-th].
- [175] N. Barnaby and M. Peloso, *Phys. Rev. Lett.* **106**, 181301 (2011), arXiv:1011.1500 [hep-ph].
- [176] T. Kobayashi, M. Yamaguchi, and J. Yokoyama, *Phys. Rev. Lett.* **105**, 231302 (2010), arXiv:1008.0603 [hep-th].
- [177] L. Senatore, E. Silverstein, and M. Zaldarriaga, *JCAP* **08**, 016 (2014), arXiv:1109.0542 [hep-th].
- [178] M. Biagetti, M. Fasiello, and A. Riotto, *Phys. Rev. D* **88**, 103518 (2013), arXiv:1305.7241 [astro-ph.CO].
- [179] V. Mandic, S. Bird, and I. Cholis, *Phys. Rev. Lett.* **117**, 201102 (2016), arXiv:1608.06699 [astro-ph.CO].
- [180] N. Bartolo, V. De Luca, G. Franciolini, A. Lewis, M. Peloso, and A. Riotto, *Phys. Rev. Lett.* **122**, 211301 (2019), arXiv:1810.12218 [astro-ph.CO].
- [181] J. F. Dufaux, A. Bergman, G. N. Felder, L. Kofman, and J.-P. Uzan, *Phys. Rev. D* **76**, 123517 (2007), arXiv:0707.0875 [astro-ph].
- [182] C. J. Hogan, *Mon. Not. Roy. Astron. Soc.* **218**, 629 (1986).
- [183] T. Vachaspati and A. Vilenkin, *Phys. Rev. D* **31**, 3052 (1985).
- [184] L. M. Krauss, *Phys. Lett. B* **284**, 229 (1992).
- [185] M. Kamionkowski, A. Kosowsky, and M. S. Turner, *Phys. Rev. D* **49**, 2837 (1994), arXiv:astro-ph/9310044.
- [186] C. Grojean and G. Servant, *Phys. Rev. D* **75**, 043507 (2007), arXiv:hep-ph/0607107.
- [187] C. Caprini *et al.*, *JCAP* **04**, 001 (2016), arXiv:1512.06239 [astro-ph.CO].
- [188] A. Mazumdar and G. White, *Rept. Prog. Phys.* **82**, 076901 (2019), arXiv:1811.01948 [hep-ph].
- [189] A. Kosowsky, M. S. Turner, and R. Watkins, *Phys. Rev. Lett.* **69**, 2026 (1992).
- [190] M. Hindmarsh, S. J. Huber, K. Rummukainen, and D. J. Weir, *Phys. Rev. Lett.* **112**, 041301 (2014), arXiv:1304.2433 [hep-ph].
- [191] M. Hindmarsh, S. J. Huber, K. Rummukainen, and D. J. Weir, *Phys. Rev. D* **92**, 123009 (2015), arXiv:1504.03291 [astro-ph.CO].
- [192] M. Hindmarsh, *Phys. Rev. Lett.* **120**, 071301 (2018), arXiv:1608.04735 [astro-ph.CO].
- [193] R. Jinno and M. Takimoto, *Phys. Rev. D* **95**, 024009 (2017), arXiv:1605.01403 [astro-ph.CO].
- [194] M. Hindmarsh, S. J. Huber, K. Rummukainen, and D. J. Weir, *Phys. Rev. D* **96**, 103520 (2017), [Erratum: *Phys. Rev. D* **101**, 089902 (2020)], arXiv:1704.05871 [astro-ph.CO].
- [195] K. Enqvist, J. Ignatius, K. Kajantie, and K. Rummukainen, *Phys. Rev. D* **45**, 3415 (1992).
- [196] J. R. Espinosa, T. Konstandin, J. M. No, and G. Servant, *JCAP* **06**, 028 (2010), arXiv:1004.4187 [hep-ph].
- [197] X. Wang, F. P. Huang, and X. Zhang, *JCAP* **05**, 045 (2020), arXiv:2003.08892 [hep-ph].
- [198] F. P. Huang and X. Zhang, *Phys. Lett. B* **788**, 288 (2019), arXiv:1701.04338 [hep-ph].
- [199] K. Kajantie, M. Laine, K. Rummukainen, and M. E. Shaposhnikov, *Nucl. Phys. B* **466**, 189 (1996), arXiv:hep-lat/9510020.
- [200] K. Kajantie, M. Laine, K. Rummukainen, and M. E. Shaposhnikov, *Phys. Rev. Lett.* **77**, 2887 (1996), arXiv:hep-ph/9605288.
- [201] P. A. R. Ade *et al.* (Planck), *Astron. Astrophys.* **571**, A25 (2014), arXiv:1303.5085 [astro-ph.CO].
- [202] A. Vilenkin and E. P. S. Shellard, *Cosmic Strings and Other Topological Defects* (Cambridge University Press, 2000).
- [203] A. Vilenkin, *Phys. Rev. D* **24**, 2082 (1981).
- [204] D. G. Figueroa, M. Hindmarsh, and J. Urrestilla, *Phys. Rev. Lett.* **110**, 101302 (2013), arXiv:1212.5458 [astro-ph.CO].
- [205] J. Giblin, John T., L. R. Price, X. Siemens, and B. Vlcek, *JCAP* **11**, 006 (2012), arXiv:1111.4014 [astro-ph.CO].
- [206] D. G. Figueroa, M. Hindmarsh, J. Lizarraga, and J. Urrestilla, (2020), arXiv:2007.03337 [astro-ph.CO].
- [207] E. Fenu, D. G. Figueroa, R. Durrer, and J. Garcia-Bellido, *JCAP* **0910**, 005 (2009), arXiv:0908.0425 [astro-ph.CO].
- [208] R. R. Caldwell and B. Allen, *Phys. Rev.* **D45**, 3447 (1992).
- [209] S. A. Sanidas, R. A. Battye, and B. W. Stappers, *Phys. Rev.* **D85**, 122003 (2012), arXiv:1201.2419 [astro-ph.CO].
- [210] A. Vilenkin, *COSMIC STRINGS AND OTHER TOPOLOGICAL DEFECTS* (1986).
- [211] M. B. Hindmarsh and T. W. B. Kibble, *Rept. Prog. Phys.* **58**, 477 (1995), arXiv:hep-ph/9411342.
- [212] N. Turok and D. N. Spergel, *Phys. Rev. Lett.* **66**, 3093 (1991).
- [213] R. Durrer, M. Kunz, and A. Melchiorri, *Phys. Rept.* **364**, 1 (2002), arXiv:astro-ph/0110348.
- [214] L. Bethke, D. G. Figueroa, and A. Rajantie, *Phys. Rev. Lett.* **111**, 011301 (2013), arXiv:1304.2657 [astro-ph.CO].
- [215] P. Auclair *et al.*, *JCAP* **04**, 034 (2020), arXiv:1909.00819 [astro-ph.CO].
- [216] Z. Arzoumanian *et al.* (NANOGRAV), *Astrophys. J.* **859**, 47 (2018), arXiv:1801.02617 [astro-ph.HE].
- [217] C. Ringeval and T. Suyama, *JCAP* **12**, 027 (2017), arXiv:1709.03845 [astro-ph.CO].
- [218] J. J. Blanco-Pillado and K. D. Olum, *Phys. Rev.* **D96**, 104046 (2017), arXiv:1709.02693 [astro-ph.CO].
- [219] B. Allen and E. P. S. Shellard, *Phys. Rev. D* **45**, 1898 (1992).
- [220] J. J. Blanco-Pillado, K. D. Olum, and B. Shlaer, *Phys. Rev. D* **89**, 023512 (2014), arXiv:1309.6637 [astro-ph.CO].
- [221] L. Sousa and P. P. Avelino, *Phys. Rev. D* **88**, 023516 (2013), arXiv:1304.2445 [astro-ph.CO].
- [222] B. P. Abbott *et al.* (LIGO Scientific, Virgo), *Phys. Rev.* **D97**, 102002 (2018), arXiv:1712.01168 [gr-qc].
- [223] Y. Cui, M. Lewicki, D. E. Morrissey, and J. D. Wells, *Phys. Rev. D* **97**, 123505 (2018), arXiv:1711.03104 [hep-ph].
- [224] S. Biscoveanu, C. Talbot, E. Thrane, and R. Smith, *Phys. Rev. Lett.* **125**, 241101 (2020), arXiv:2009.04418 [astro-ph.HE].
- [225] G. Boileau, N. Christensen, R. Meyer, and N. J. Cornish, *Phys. Rev. D* **103**, 103529 (2021), arXiv:2011.05055 [gr-qc].
- [226] I. Kowalska, T. Bulik, K. Belczynski, M. Dominik, and D. Gondek-Rosinska, *Astron. Astrophys.* **527**, A70 (2011), arXiv:1010.0511 [astro-ph.CO].
- [227] C. L. Rodriguez, S. Chatterjee, and F. A. Rasio, *Phys.*

- Rev. D **93**, 084029 (2016), [arXiv:1602.02444 \[astro-ph.HE\]](#).
- [228] F. Antonini and H. B. Perets, *Astrophys. J.* **757**, 27 (2012), [arXiv:1203.2938 \[astro-ph.GA\]](#).
- [229] M. Colpi and A. Sesana, “Gravitational Wave Sources in the Era of Multi-Band Gravitational Wave Astronomy,” in *An Overview of Gravitational Waves: Theory, Sources and Detection*, edited by G. Auger and E. Plagnol (2017) [arXiv:1610.05309 \[astro-ph.HE\]](#).